The United Nations University

GEOTHERMAL TRAINING PROGRAMME
Orkustofnun, Grensásvegur 9,
IS-108 Reykjavík, Iceland

Reports 1995
Number 11

ONE- AND TWO-DIMENSIONAL INTERPRETATION OF DC-RESISTIVITY DATA FROM THE BERLÍN GEOTHERMAL FIELD, EL SALVADOR

Pedro Antonio Santos López
Comisión Ejecutiva Hidroeléctrica del Río Lempa (C.E.L.),
Centro de Investigaciones Geotérmicas (C.I.G.),
km 11 1/2 Carretera la Puerto La Libertad,
Santa Tecla, La Libertad,
EL SALVADOR, C.A.

ABSTRACT

The results of the interpretation of 50 resistivity soundings carried out in the Berlín geothermal field delineate an extensive geothermal field of 12 km^2 at 250 m below sea level. The field is characterized by a low-resistivity cap which is underlain by a high-resistivity core where temperatures exceed 230°C, providing there is an equilibrium between temperature and alteration. The upflow zone is within the caldera close to well TR-5. This is supported by the highest measured temperatures and highest elevation of the high-resistivity core. The existence of a high-resistivity core suggests a fresh water system in the uppermost part of the reservoir, or at least at the depths where resistivity data is dependable.

1. INTRODUCTION

El Salvador is located on the southern coast of Central America, where the Cocos plate is subducting underneath the Caribbean plate, forming an E-W tectonic graben. On the southern margin of this graben lies the Quaternary volcanic chain. Seven high-temperature geothermal fields (280-320°C) have been identified lying on the northern flanks of this volcanic chain (Figure 1). The Berlín geothermal field is situated 100 km east of the capital city San Salvador, associated with the Tecapa volcanic group and the Berlín caldera, which is of Pleistocene age (Pullinger and Bruno, 1995).

The geothermal exploration began in 1966 with the investigations carried out by the United Nations Development Programme (UNDP). During this stage, two shallow wells and well TR-1 were drilled revealing a commercially exploitable geothermal reservoir at depth (Monterrosa, 1993). During 1978-1981 five additional wells were drilled with a proven potential of 24 MW. With the assistance of Electroconsult (ELC), a feasibility study was made which proved to be positive and encouraged more geoscientific investigations and development of the resource.

In 1977 the first DC resistivity survey was done by the Comisión Ejecutiva Del Río Lempa (CEL) completing a total of 78 soundings (Schlumberger array). In 1993, Electroconsult started scientific

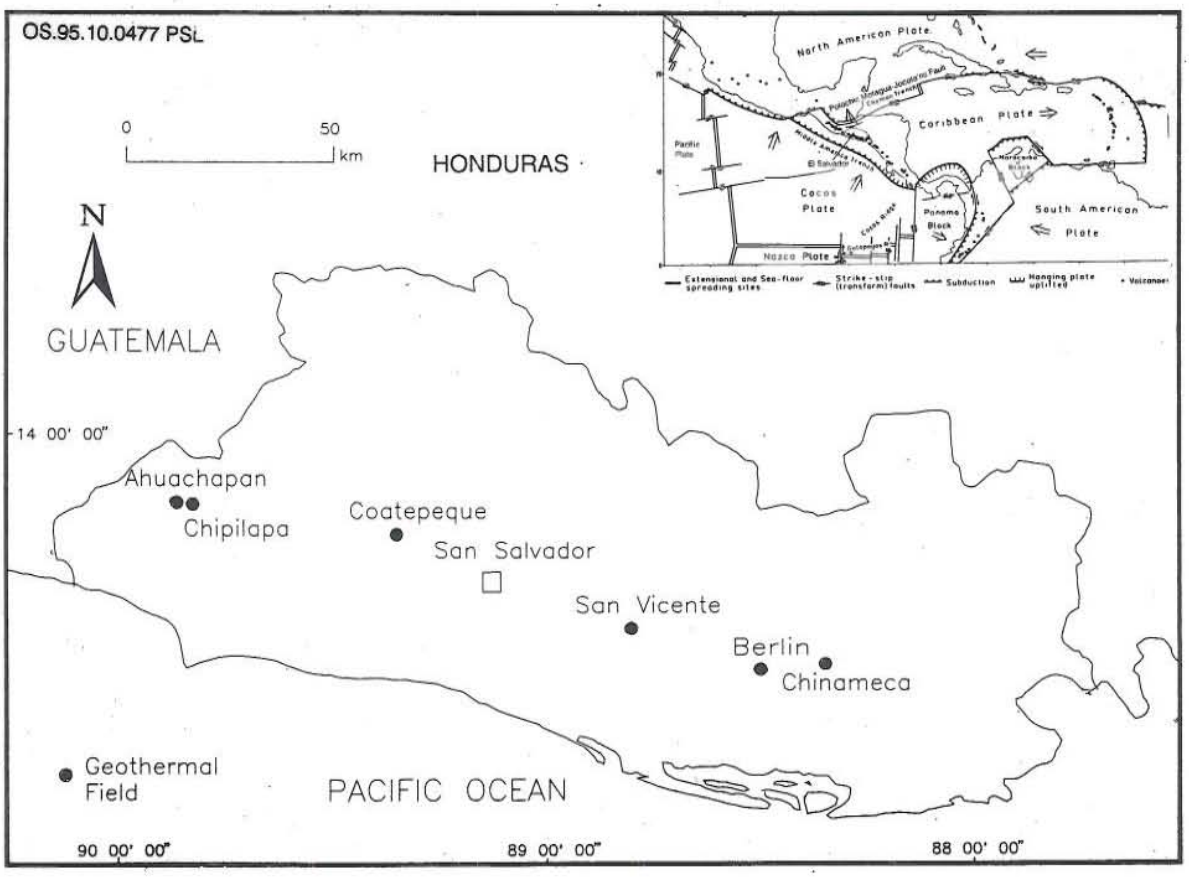

FIGURE 1: High-temperature geothermal fields in El Salvador (Quijano, 1994), inset is the regional tectonic map (Weyl, 1980)

investigations to assess the feasibility for the installation of a condensing power plant with the capacity of 50 MW. In March-June 1994 Geothermal Energy New Zealand Ltd (GENZL, 1994) conducted geological investigations and a magnetotelluric survey. These studies confirmed the extension of the field south of the actual production area. In July-October the same year, a DC resistivity survey was carried out (Schlumberger array). In total 41 sounding stations were measured, distributed on a regular grid with a density of one sounding per km^2, and a maximum current electrode spacing between 2000 and 4000 m.

This report contains the results from the interpretation of 40 DC resistivity soundings done in 1994 and 10 from the 1977 resistivity survey. The results of both one- and two-dimensional interpretation are correlated with the information obtained from the wells. The report also presents a brief outline of the Berlín geothermal field, as well as a theoretical overview of DC Schlumberger sounding method, methods of interpretation and the main factors affecting the data acquisition.

2. BERLÍN GEOTHERMAL FIELD

2.1 Geological and structural setting

The subduction of the Cocos plate under the Caribbean plate has formed a tectonic graben that runs E-W through El Salvador. Berlín volcano appears to be centred where the regional northwest trending fault

system intersects the southern margin of the E-W trending fault system forming the 5 km wide Berlín graben. The forming of the large basaltic andesite composite cone during the last 1-2 million years was interrupted twice by the last explosive andesite eruptions forming black and grey ignimbrites. These eruptions were accompanied by a collapse of the upper part of the central cone, controlled partly by the previous existing northwest trending faults, and forming the outlines of the Berlín caldera (GENZL, 1995).

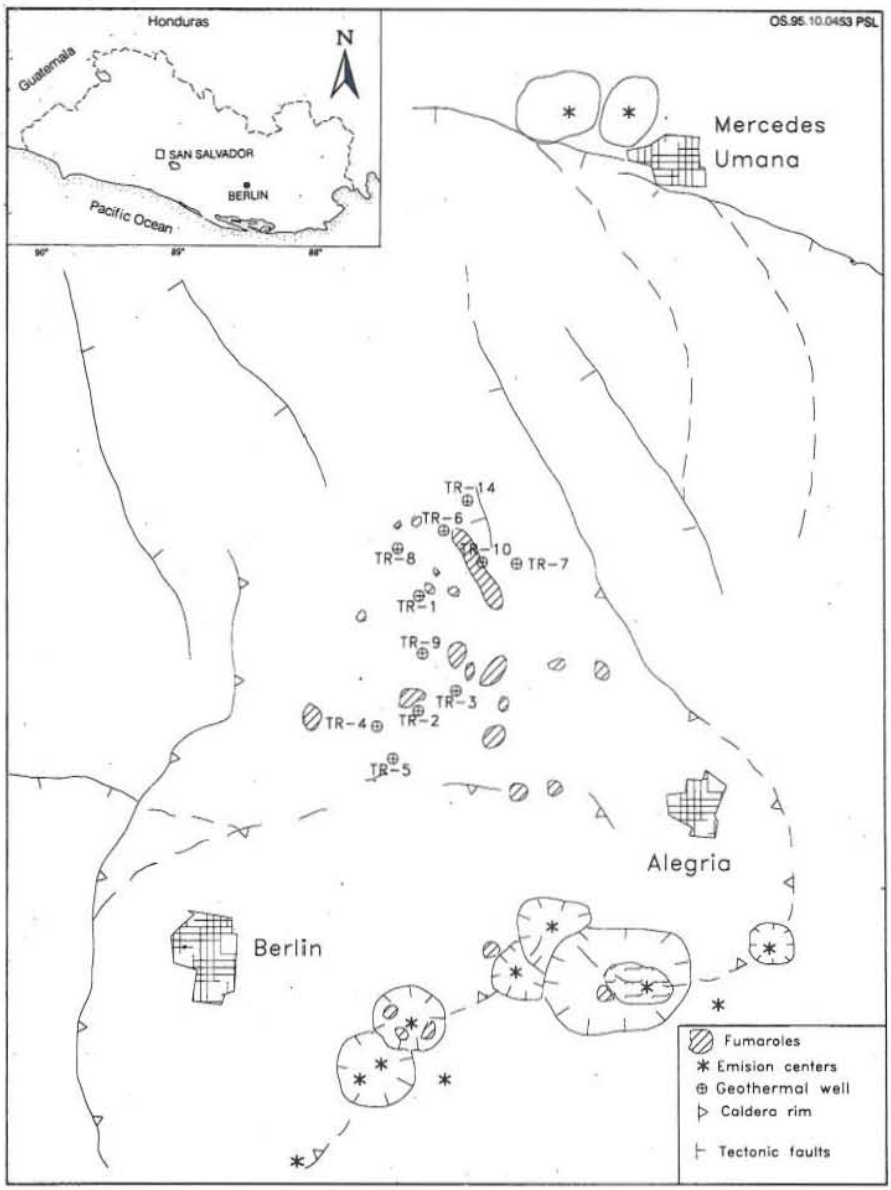

FIGURE 2: Geological structures of the Berlín geothermal field and geothermal manifestations (modified from Pullinger and Bruno, 1995)

The northwest graben cuts through the northern part of this caldera, and it is believed that the faults along with the conjugated northeast faults transport the geothermal fluid from the upflow zone close to the young craters towards the wellfield. This fluid is discharged at several hot springs close to San Simon and Lempa rivers, shown on the structural geological map in Figure 2 (Pullinger and Bruno, 1995).

Several fumaroles and hot springs are aligned to the younger transverse fault system with NNW-SSE orientation related to the caldera collapse. The rocks derived from the collapse of the caldera walls are probably included in the lithic lag breccias seen in the grey ignimbrites deposits surrounding the caldera.

The volcanic activity continued within the preexisting caldera where small intra-caldera eruptive centres were formed, some of them dating approximately 0.22 to 0.1 million years back, where basaltic lavas and scoria were emitted. A plinian eruption of big magnitude took place 75,000 years back emitting 5-10 km^3 of coarse lithic clasts and plinian basalt pumice fall deposits (Blanca Rosa). The distribution of the isopaches suggests that the source of this eruption is in the northern part of the Berlín caldera. The subsequent effusive and explosive volcanic activity from the intra-caldera centres produced basaltic

andesitic lavas. This activity continued until about 700 years back according to radiometric dates (GENZL, 1995)

2.2 Geochemistry and temperature distribution

Fluid samples collected from the wells and measured temperatures indicate that Berlín geothermal field is a liquid dominated system with temperatures ranging from 300-320°C. The fluids discharged from the reservoir are classified as sodium-chloride type with an intermediate chloride concentration of 3000-5000 ppm and neutral sodium-chloride. The gas concentration is relatively low, with gas/steam ratio less than 150, and the salinity between 7000 and 1200 ppm (Monterrosa, 1993).

According to the chemical analysis, three types of aquifers have been identified; a shallow aquifer with low salinity of 1600 ppm between 200-300 m a.s.l.; the second aquifer at sea level depth with intermediate salinity of 6600 ppm; and a deeper saline aquifer of 8000-12000 ppm at -800 to -1200 m a.s.l. (CEL, 1991).

The chemical information in the area of the natural activity and the discharge of the wells suggest that the size of the geothermal system is in the range of 20-25 km^2. The geothermometry of the gases and solutions, the proportional content of gases in the fumaroles and the chloride/temperature/enthalpy indicate that the field extends southwards from the actual production zone. The changes in the chemistry of the wells suggest that the rocks of the reservoir have low to intermediate permeability (GENZL, 1995).

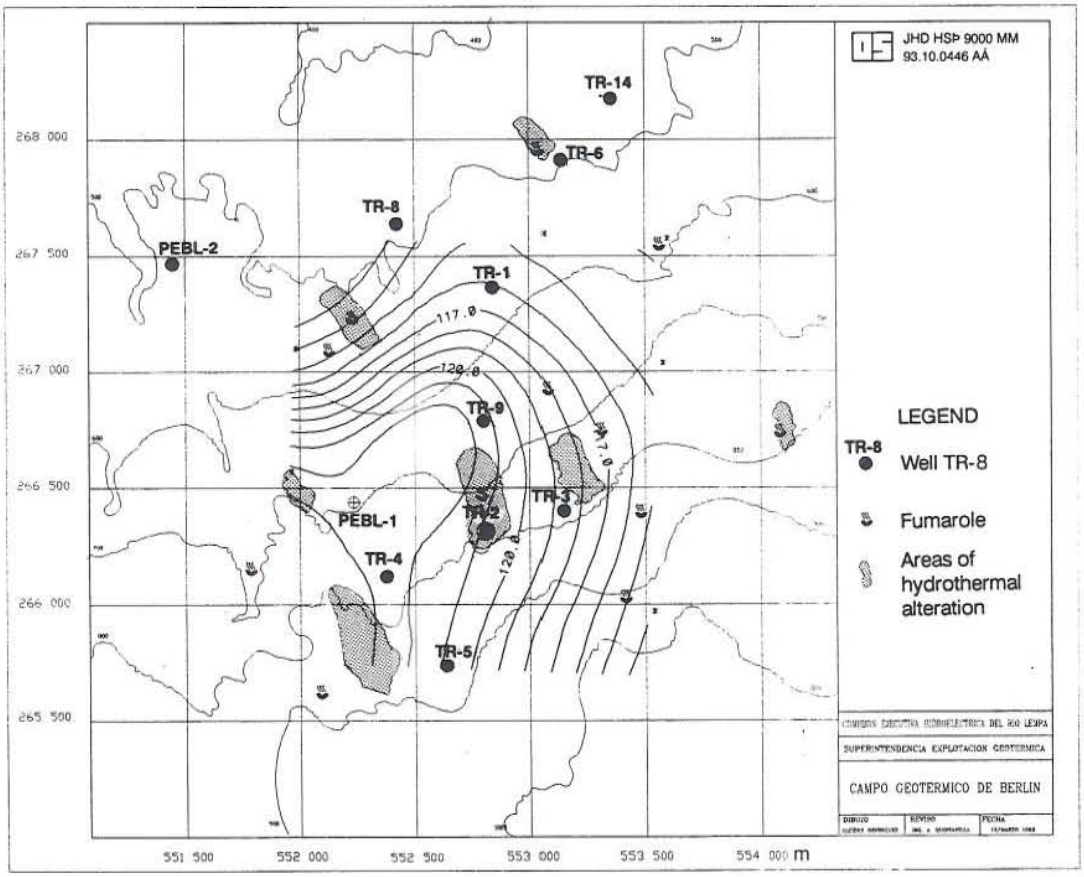

FIGURE 3: Map of the temperature distribution at 1000 m below sea level in the Berlín geothermal field (Monterrosa, 1993)

The temperature registered in the wells of Berlín geothermal field has been analysed by Electroconsult (ELC, 1993) and by Monterrosa (1993) as a project of the UNU Geothermal Training Programme. About 274 temperature logs had been carried out in the 8 wells since 1978, with a depth range of 1500-2300 m. Conclusions drawn from these studies are summarized as follows:

a) Measurements from wells TR-1, TR-3, TR-4 and TR-5 show clearly a relative maximum of temperature (150-200°C) at -300 to +400 m a.s.l. related to a hot shallow aquifer. This is not clearly evident in wells TR-2 and TR-9;
b) The temperature recorded in well TR-1 is lower than in the other wells, indicating that it is situated in a low-permeability area;
c) The maximum temperatures registered are between 295 and 305°C at a depth range of -800 to -1200 m a.s.l. According to analysis of the pivot point from pressure logs, the main feed zone is located at this depth;
d) All of the temperature logs (except in TR-1) show an inversion phenomenon at the bottom with a decrease in temperature of 5-20°C. This is associated with a horizontal fluid flow, initially towards northeast and later on to a north-northwesterly direction;

The temperature distribution at -1000 m a.s.l. shown in Figure 3 indicates a tendency of temperature decrease towards the north-northwesterly part of the wellfield with a gradual increase to south and southwest identifying a possible upflow zone. This tendency is underlined in the N-S temperature cross-section in Figure 4.

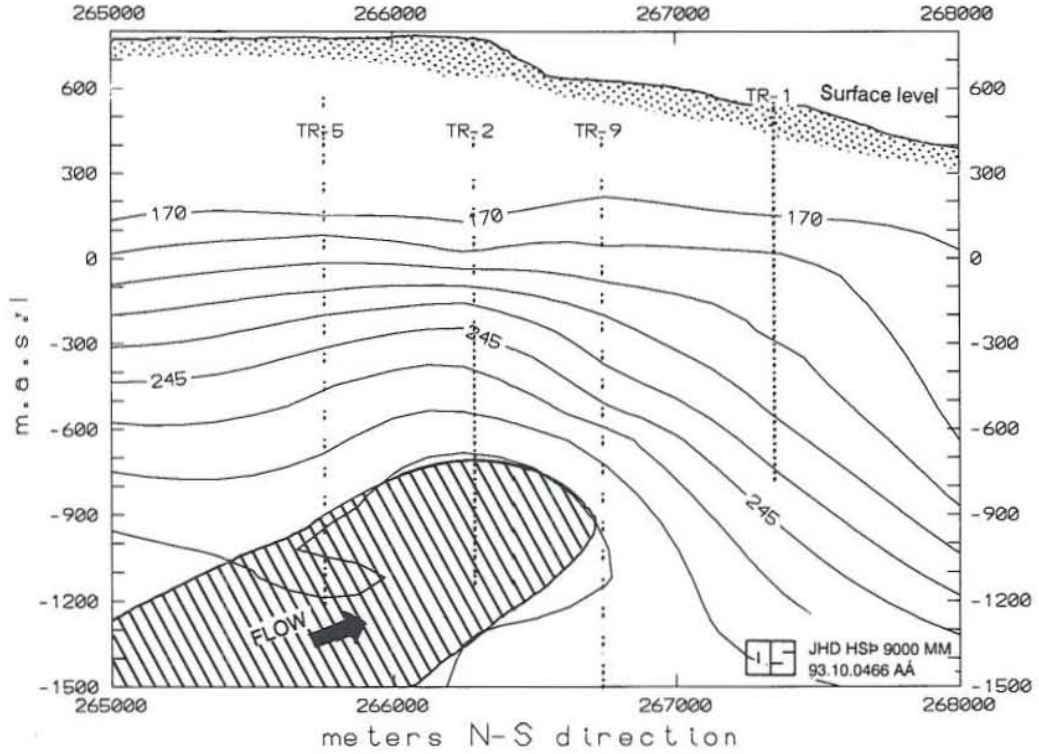

FIGURE 4: A N-S temperature cross-section through the Berlín geothermal field (Monterrosa, 1993)

2.3 Alteration mineralogy

Due to the seepage of geothermal fluids through the rocks, original glass and minerals are replaced by secondary minerals which also fill the pores and cracks in the rocks. The rate of alteration is dependent

on many factors such as temperature, chemistry, lithology and permeability, which are critical factors for the alteration progress. The flow through the rocks is governed by the tectonic pattern. The interpretation of the thermal history of altered rocks from their mineralogy is of a potential use. A fossil geothermal gradient can be determined and the development of a geothermal area can be reconstructed (Kristmannsdóttir, 1978).

The mineralogy of alteration characterized in Berlín geothermal field has been studied by Electroconsult (ELC, 1993), the Instituto de Investigaciones Eléctricas (IIE, 1992) and CEL. The techniques applied for the determination of minerals are basically analyses through petrographic microscope and diffraction of X-rays. The primary mineralogy associated with the subsurface lithology distribution is determined by petrography according to IIE and summarized in Table 1.

TABLE 1: Primary mineralogy of Berlín geothermal field

Rock type	Primary minerals identified
Basalt	Labradorite, bytownite, augite, hypersthene and pigeonite.
Andesitic-basalt	Labradorite, andesine, augite and hypersthene
Andesites	Andesine, augite and hypersthene
Lithic tuff	Rock fragment, clay and glass
Pumice	Glass

Generally the hydrothermal alteration of the Berlín geothermal field is characterised by a mixture of secondary minerals shown in Table 2. According to Kristmannsdóttir (1985) the clay minerals are qualitatively the most common and voluminous alteration minerals, responding easily to changes in temperature and physical conditions and are therefore an important indicator of stability. An examination of the clay minerals and their relation to other minerals is very useful for the interpretation of the thermal history of a geothermal field.

TABLE 2: Secondary minerals identified in the Berlín geothermal field

Group	Secondary minerals
Silica	Quartz, chalcedony and opal
Chlorites	Clinochlor, prochlorite and penninite
Carbonates	Calcite
Calc-silicates	Zeolites, epidote sulphates and micas
Oxides	Magnetite, hematite
Sulphides	Pyrite

The mineralogical facies are defined based on the empirical relation between the rock formation temperatures measured from the wells and the alteration temperature of the secondary minerals. The mineralogical facies as a function of the temperatures from Berlín geothermal field are described by Pullinger and Barrios (1994) in the report "Evaluación de informacion geocientifica de pozos TR-14 y TR-8". The results are summarized in Table 3. The range of temperature specified are referred to as the stabilization temperatures of the secondary minerals and the depth range shows the depth of identification of the minerals in the northern and southern part of the geothermal field respectively. The thickness and the lower limit of prophilithic facies has not been identified.

TABLE 3: Classification of mineralogical facies of Berlín geothermal field (Pullinger and Barrios, 1994)

Facies	Characteristic minerals	Temperature range (°C)	Depth range (m a.s.l.)	Average thickness (m)
Argillic	Clay minerals: Zeolite and smectite type	50-150	500 to 150	400
Phyllic-argillic	Clay mineral type chloritic: Zeolite, quartz, calcite	150-180	100 to -100	400
Phyllic	Diminution clay mineral and traces of chlorite	180-200	-400 to -700	600
Phyllic-prophylithic	Chlorite group (type pennite) and epidote traces	200-230	-950 to -1200	300
Prophylithic	Epidote	230-250	-1200 to ?	?

2.4 Previous geophysical studies

Geophysical exploration started in 1977 with a DC resistivity and a gravity survey, carried out by CEL. The exploration studies continued until 1994 with a magnetotelluric and DC resistivity survey conducted by GENZL and CEL, respectively. The DC resistivity survey carried out in 1977 in the northern part of the geothermal field, consisted of 78 soundings with Schlumberger array and current electrode distance up to 2000 m, using a 0.3 Hz DC transmitter of McPhar type, model 503E.

The results of the reinterpretation of the gravity and resistivity data done by Electroconsult (ELC, 1993), indicate a positive gravimetric anomaly in the central part of the field, possibly due to the presence of a deep dense body or the progressive alteration of the rocks. The negative anomaly appears in the north part of the field. A low-resistivity layer of 10-25 Ωm is at 100-400 m depth with NNW-SSE direction. A clear correlation was observed between the results of both methods in the central and northwest part of the field where the dipping of resistivity layers is coherent with the diminution of the gravity anomaly. This correlation was not possible to establish in the southern part of the field due to the strong differences between the results of the two methods. Therefore, more geophysical studies were recommended towards the southern part of the field using methods with the capacity to probe deeper such as magnetotelluric (MT) soundings (ELC, 1993).

The magnetotelluric survey was conducted by GENZL in 1994, confirming the extension of the production field towards south and southeast. The low-resistivity values in the north were explained as traces of alteration from an old geothermal system. The conductive layer was pretty well defined showing lower values in the southern part. The limits of these thin layers were associated with the north-northwest part of the graben which cuts the caldera in the south part (GENZL, 1995).

The resistivity features put wells TR-8 and TR-14 at the margin north of the geothermal field. A DC resistivity survey was carried out in July-October 1995. Schlumberger array with 41 soundings regularly distributed in a grid of 36 km^2 with relative separation of about one kilometre between the soundings and the current electrode spacing (AB) extending to 2000-4000 m. The results of one- and two-dimensional interpretation of these soundings are presented in Chapter 4.

3. DC SCHLUMBERGER SOUNDINGS

Direct current resistivity measurements have been used to obtain quantitatively, from data registered at the earth's surface, the changes in resistivity distribution with depth. They have been widely and successfully used for detection and delineation of geothermal resources, location of aquifers, etc. The application of the different resistivity methods during the exploration of a geothermal field depends on the geological structure of the field and the information desired.

The basic principle of DC resistivity methods is to inject a known current into the earth through current electrodes at the surface, creating a potential field in the earth. The subsurface resistivity can be inferred by measuring the resulting potential differences.

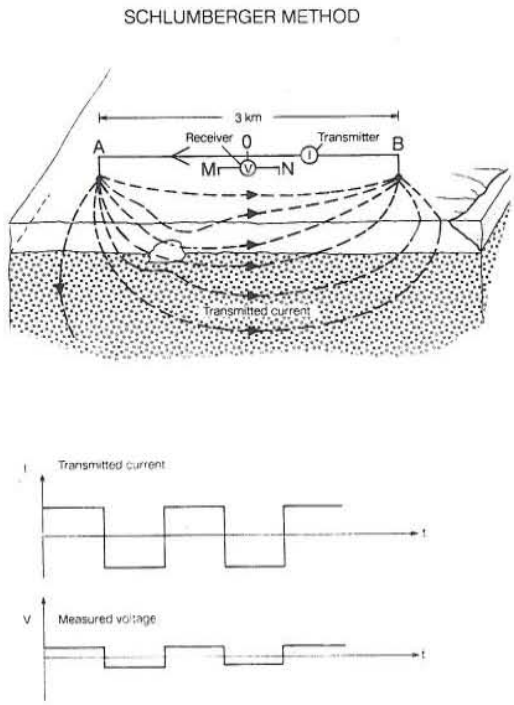

FIGURE 5: The Schlumberger sounding configuration (Hersir and Björnsson, 1991)

DC resistivity methods can be divided into various subcategories depending on the geometrical arrangement of electrodes. The most common are Schlumberger sounding, dipole sounding and head-on profiling. The main disadvantages of these methods are their sensitivity to lateral inhomogeneities and limited capacity of depth prospection (<1500 m). DC Schlumberger sounding in combination with head-on profiling have been applied in Iceland for detailed structural analysis of the uppermost kilometre of the earth's crust (Flóvenz, 1984).

3.1 Theoretical background

In the Schlumberger array four electrodes are symmetrically positioned along a straight line with the current electrodes, A and B, on the outside and the potential electrodes M and N on the inside of the array (Figure 5). The current I is injected into the ground through A and B and the resulting potential, ΔV difference between M and N measured. The apparent resistivity, ρ_a, can then be calculated according to the formula

$$\rho_a = \frac{\Delta V}{I} \frac{\pi(S^2 - P^2)}{2P} \qquad (1)$$

where S = AB/2 (m) and P = MN/2 (m).

In order to able to interpret the measured apparent resistivity in terms of theoretical models, a general expression for the potential due to a current source at the surface is needed. The following theoretical discussion shows the main steps towards that goal. For further information refer to e.g. Koefoed (1979), Hersir and Árnason (1989) or Reyes (1989). Only simple one-dimensional models will be considered. This means that it is assumed that the earth consists of n different resistivity layers, each layer i with a resistivity ρ_i, thickness d_i and depth to the lower boundary h_i. The bottom layer has the resistivity ρ_n and infinite thickness.

The current distribution and electrical field are related by Ohm's law

$$\vec{J} = \frac{\vec{E}}{\rho} \tag{2}$$

where

$\vec{E}$ = Electrical field (Volt/m);
$\vec{J}$ = Current density (A/m^2);
ρ = Resistivity (Ωm)

The divergence of the current density in a given volume is equal to the difference in the current flow into and out of the volume, which is equal to zero except at a current source and current sink. Therefore, the divergence is equal to zero throughout the half space except at source points at the surface where it is given by

$$\nabla \vec{J} = I\delta(\vec{x}) \tag{3}$$

where $\delta(x)$ is Dirac delta function.

The electric field, $\vec{E}$, is defined as the negative gradient of the potential, V

$$\vec{E} = -\nabla V \tag{4}$$

From Equations 2, 3 and 4 and for the uppermost layer where $\rho=\rho_1$, then

$$-\nabla^2 V = \rho_1 I\delta(\vec{x}) \tag{5}$$

which is an inhomogeneous differential equation of second order. A special solution in cylindrical coordinates is given by

$$V(r,z) = \frac{\rho_1 I}{2\pi}\int_0^\infty e^{-\lambda z} J_o(\lambda r)\, d\lambda \tag{6}$$

where J_o is the Bessel function of order zero.

This solution is only valid for the uppermost layer. For all other layers $\nabla\vec{J}= 0$, or

$$\frac{\nabla^2 V}{\rho_i} = 0 \qquad i.e. \qquad \nabla^2 V = 0 \tag{7}$$

This is the Laplace equation. The general solution of the homogeneous equation within each layer, i, is given by

$$V_i = \int_0^\infty [C_i(\lambda) e^{\lambda z} + D_i(\lambda) e^{-\lambda z}] J_0(\lambda r)\, d\lambda \qquad (8)$$

for $i = 1, 2,...,n$. $C_i(\lambda)$ and $D_i(\lambda)$ are functions of the arbitrary constant λ.

The general solution for the inhomogeneous differential equation of second order (Equation 5) for the uppermost layer (i = 1) can be written as a sum of the general solution of homogeneous equation (Equation 8) and the special solution given by Equation 6

$$V_i = \frac{\rho_1 I}{2\pi} \int_0^\infty [e^{-\lambda z} + k_i(\lambda) e^{-\lambda z} + h_i(\lambda) e^{\lambda z}] J_0(\lambda r)\, d\lambda \qquad (9)$$

where

$$k_1(\lambda) = 2\pi D_1(\lambda) / \rho_1 I \qquad \text{and} \qquad h_1 = 2\pi C_1(\lambda) / \rho_1 I$$

For the other layers, $i > 1$, the solutions can be written in the same form by defining (for i > 1)

$$k_i(\lambda) = 2\pi D_i(\lambda) / \rho_1 I \qquad \text{and} \qquad h_i(\lambda) = 2\pi C_i(\lambda) / \rho_1 I$$

The task is now to determine the functions $k_i(\lambda)$ and $h_i(\lambda)$. That can be done by imposing boundary conditions for the potential V which are the following:

1. The potential is continuous at each of the boundary planes between layers; $V_i = V_{i+1}$;
2. The vertical component of the current density J_i is continuous across the boundaries of layers, i.e.: $J_i(z) = J_{i+1}(z)$; where $J(z) = (\partial V/\partial z)/\rho$ at $z = h_i$
3. At the surface, $z = 0$, the vertical component of the current density $J(z)$ is zero and consequently the electrical field, except at the current source.
4. The potential vanishes at infinity, i.e. $V \to 0$, when $z \to \infty$ or $r \to \infty$.

Considering the 4th boundary condition for the bottom layer ($i = n$) $h_n(\lambda) = 0$, hence, for that layer Equation 9 can be written as

$$V_n = \frac{\rho_1 I}{2\pi} \int_0^\infty [1 + k_n(\lambda)] e^{-\lambda z} J_0(\lambda r)\, d\lambda \qquad (10)$$

Using the 3rd boundary condition (differentiating Equation 9 with respect to z and demanding it to be 0 at Z = 0), it can be shown that for the uppermost layer (i=1) Equation 9 becomes

$$V_1(r) = \frac{\rho_1 I}{2\pi} \int_0^\infty [1 + k_1(\lambda) e^{-\lambda z} + k_1(\lambda) e^{\lambda z}] J_0(\lambda r)\, d\lambda \qquad (11)$$

Solving for the case of two layers, i.e. using Equation 12, and $V_n = V_2$ in Equation 10. Applying the 1st

boundary condition gives $V_1(h) = V_2(h)$. Taking the derivatives of the potential with respect to z, at $z = h$, and applying the 2nd boundary condition, it can be shown that $k_i(\lambda)$ known as Stefanescu's Kernel function is

$$k_1(\lambda) = \frac{\kappa_1 e^{-2\lambda h}}{1 - \kappa_1 e^{-2\lambda h}} \tag{12}$$

where

$$\kappa_1 = \frac{\rho_2 - \rho_1}{\rho_1 + \rho_2} \tag{13}$$

Equation 11 can be rewritten as

$$V(r) = \frac{\rho_1 I}{2\pi} \int_0^\infty J_0(\lambda r)\, d\lambda + \frac{\rho_1 I}{\pi} \int_0^\infty k_1(\lambda) J_0(\lambda r)\, d\lambda \tag{14}$$

It can be shown that for the Bessel function of order zero J_0 the following is valid at the surface, z=0:

$$\int_0^\infty J_0(\lambda r)\, d\lambda = \frac{1}{r} \tag{15}$$

Hence, Equation 14, giving the potential at the surface, can be written as

$$V(r) = \frac{\rho_1 I}{2\pi r} + \frac{\rho_1 I}{\pi} \int_0^\infty k_1(\lambda) J_0(\lambda r)\, d\lambda \tag{16}$$

where

V	= Potential at a point on the surface a distance r from the source;
I	= Current intensity at a point source;
ρ_1	= Resistivity of the uppermost layer;
λ	= Integral variable
r	= Distance between the current source and potential source
$J_0(\lambda r)$	= Bessel function of order zero
$k_1(\lambda)$	= Stefanescu's Kernel function dependent on the layer parameters ρ_i and h_i

For the case of n layers and with $K = 1 + 2k(\lambda)$, the general potential equation at the surface is given by

$$V_{(r,z=0)} = \frac{\rho_1 I}{2\pi} \int_0^\infty K_i(\lambda) J_0(\lambda r)\, d\lambda \tag{17}$$

where

$$K_i = \frac{K_{i+1} + \frac{\rho_i}{\rho_{i+1}} \tanh(\lambda d_i)}{\frac{\rho_i}{\rho_{i+1}} + K_{i+1} \tanh(\lambda d_i)} \tag{18}$$

In practice the distance between the potential electrode is much smaller than between the current electrodes. Assuming that the potential changes linearly between the potential electrodes, the potential difference is found by differentiating V

$$\frac{\Delta V}{2P} = -2\left[\frac{\partial V}{\partial r}\right]_{r=S} \tag{19}$$

This is called the gradient approximation and the apparent resistivity is now given by

$$\rho_a = \rho_1 + 2\rho_1 S^2 \int_0^\infty k_1(\lambda) J_1(\lambda S)\, d\lambda \tag{20}$$

By using this approximation it becomes necessary to tie in the different segments of the sounding curve to get a continuous curve for interpretation, which is the most common method for one-dimensional interpretation of Schlumberger soundings.

3.2 Field work and instrumentation

A resistivity survey starts with the pre field work, evaluating all the requirements and the possible obstacles that may affect the fieldwork wasting valuable time at the site. In the elaboration of the budget, factors like manpower required, transportation, equipment, accommodation, rate of work per day, time and the assessment of total cost of the collected data must be considered.

Choosing the site. The effects of lateral inhomogeneities formed by roads, ditches, wire fences, buried pipelines and rail roads on measurements must be kept in mind when choosing the site of a resistivity sounding and in particular in choosing positions of the potential electrodes. The effects of these inhomogeneities distort the pattern of the current flow, altering the potential difference measured. Therefore the position of the potential electrodes must be kept at a safe distance from lateral inhomogeneities (Koefoed, 1979). Inhomogeneities located near current electrodes are less harmful, they distort the current pattern only in their immediate neighbourhood. Owing to high conductance, wire fences and buried metal pipelines or wires can cause large errors in the measurements.

Field procedure. After the selection of a site and direction of the sounding, the instruments are connected. The current is then injected into the ground and the resulting potential difference (ΔV) is measured. The apparent resistivity is calculated and plotted on a bilogarithmic paper as a function of the half space of current electrodes (AB/2=S). The distance between the current electrodes is increased stepwise and distributed on a logarithmic scale with ten points per decade while keeping the distance between the potential electrodes fixed, thus obtaining information on the resistivity at greater depth. As

S increases, ΔV becomes lower. Therefore it may become necessary to increase the distance between the potential electrodes (P) to increase the signal, but keeping the relation P≤S/5. The resulting curve is hence composed of segments, one for each P. This will be discussed in Section 3.3. At least three overlapping points should be between segments in order to indicate the presence of possible lateral inhomogeneities.

Some initial judgement on the quality of the data collected must be carried out in the field. Any values that are obviously out of step should be repeated removing the error source. Good data is essential for the reliability of the sounding. Going through costly and time consuming modelling with poor data is a waste of money and time.

Instrumentation. The choice of instruments depends on the purpose of the survey (vertical resolution required), the technical specifications and the cost of the equipment, the condition of terrain and the crew available. The basic instrumentation required for a DC Schlumberger sounding consists of a DC current transmitter, receiver, power source (generator or battery), electrodes and wires, as is shown in Figure 6. The receiver is a voltmeter with a high input impedance (10^6 ohm) and the sensitivity of the order of micro-volts.

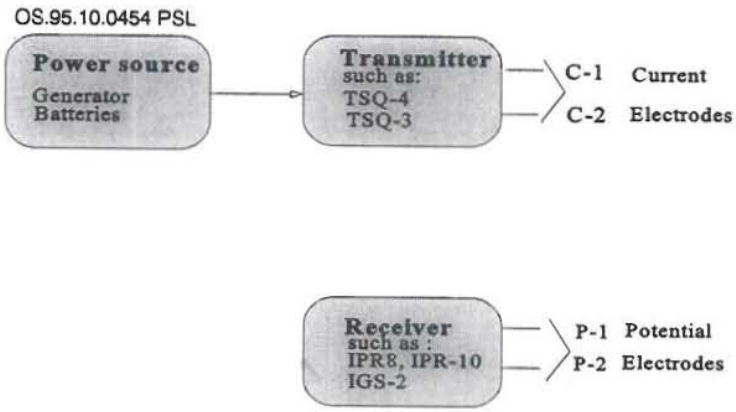

FIGURE 6: Block diagram showing examples of basic instruments needed for Schlumberger sounding

3.3 Factors that affect the data acquisition

Distortion of the sounding curves and scattering of the apparent resistivity can often be related to the conduct of the survey and is usually too late to correct once the field work has been completed. Detection of these distortions requires knowledge of the possible causes, such as the instrumentation, data acquisition or disturbance of the electrical field at the centre. These errors can be corrected by repeating the measurement. However the jump in some segments of the curve, normally found in geothermal areas may reflect the true condition beneath the surface and must be taken into account in the interpretation (Benito, 1991). The most common factor that affects the data acquisition are:

Topographic effect
It is inherent to the relative location of the current and potential electrodes and the natural conditions of the terrain itself. When the potential electrodes are placed perpendicular to the axis of a steep valley, the measured potential will be erratically different compared to that measured over a horizontal free surface. The convergence of equipotential lines in the valley will cause higher ρ_a values and divergences over the high angle ridges will cause lower ρ_a values.

Skin effect
When a wire is carrying an alternating current or, in general, any current whose magnitude is varying, the current has a tendency to dense toward the surface of the wire. The result will be a reduction in the inductance and an increase in the electric resistance of the conductor. This effect is harmful when AC current sources are used as the current density decreases exponentially with depth. The curve of the

sounding can take steep upturns of at least 45° if an AC source is utilized at the spacing of AB/2=100 m with a low-resistivity body beneath at 100-200 m depth (Hochstein et al., 1982). This effect is less harmful when a DC current source is used.

Electric coupling
Current leakages are caused by electromagnetic interference between the potential and the current circuit. The electric coupling is increased when the cables for the current are placed too close to the potential cables or when these are crossed. This effect can be reduced by keeping a distance of at least three metres between the current and potential circuits wires, and especially by using coaxial wires for the latter.

Near-surfaces inhomogeneities
In Section 3.2 it is mentioned that the ρ_a curve obtained in Schlumberger sounding is composed of shifted segments. According to Árnason (1984) these shifts are found to be in two categories "converging shifts" and "non-converging shifts". The converging shifts are caused by large resistivity contrasts between the layers in horizontally stratified earth. These shifts contain information on the resistivity structure. They are greatest when the distance *S-P* is of the same order of magnitude as the depth down to the boundary between the layers and they increase with increasing resistivity contrasts. The non-converging shifts, are caused by inhomogeneities, lateral resistivity variation, at the centre of the Schlumberger array, deforming the current and potential distribution in the vicinity of the potential electrodes. The apparent resistivity is strongly dependent on P and great shifts will appear in the apparent resistivity curve when P is changed. This phenomenon can be a considerable source of error (Árnason, 1984).

Telluric and cultural currents
There is always a flow of electrical current in the ground, also when no current is injected through electrodes. These parasitic currents are partly caused by natural (telluric currents) and man-made structures. The telluric currents are caused by the interaction between the earth's and sun's magnetic fields, and the magnitude is dependent on the sun´s activity. The occurrence of thunder storms increases this kind of noise (Ward and Sill, 1983). The cultural current noise is caused mainly by current leakage from the grounded structures such as industrial installations, rail roads, wire fences, etc. As a consequence, the potential measured is only partly due to the current injected by the current electrodes, the other part is due to the parasitic currents. Particularly at large distances between the current electrodes the signal of these parasitic current can be stronger than the signal of the current injected.

This effect is reduced by the use of a spontaneous potential compensating circuit that cancels out the DC component of the parasitic current and a lowpass filter circuit that smooths the potential difference signal by eliminating the AC component of the parasitic current.

3.4 Interpretation methods

The objective of the one-dimensional resistivity interpretation is to delineate the resistivity variation with depth assuming that the earth is electrically homogeneous and the resistivity only varies with depth, without any lateral variation. Several methods of interpretation have been developed; the older ones based on a pre-calculated catalogue of master curves (auxiliary point method), but more recently based on trial-and-error or optimization approaches etc. with the aid of computers. A closer approximation can be achieved using a one-dimensional inversion programme. A still better approximation can be achieved by using a two-dimensional interpretation, as discussed below.

One-dimensional interpretation, the SLINV programme

The SLINV programme (Árnason and Hersir, 1988) is a non-linear least-squares inversion programme using a Levenberg-Marquardt inversion algorithm together with a fast forward routine based on a linear filter method. It automatically adjusts the curve. The information obtained from the field work (volt, current, AB/2, MN/2) is used to construct an apparent resistivity curve. The different shifts, presented in the curve, must be corrected prior to the automatic process. This can be done by hand or using the PSLINV programme (developed at Orkustofnun, Iceland), the constant shift can be corrected by fixing the segment of the curve measured with the largest potential electrode distance (P) used in the sounding, and thus correct the other segments. Figure 7 shows a simplified diagram summarizing the one-dimensional interpretation process. The corrected curve is fed into the programme, as well as an initial model (guess given by the interpreter) with a fixed number of layers and initial layer parameters ρ_i and d. Using these parameters the Kernel function is calculated and the corresponding apparent resistivity values are determined by the evaluation of Equation 17 from Section 3.2. With the help of the linear method, the calculated curve is compared with the measured one, and the computer changes the layer parameters until a good fit is achieved. If the fit is not good enough the number of layers can be changed and the process repeated.

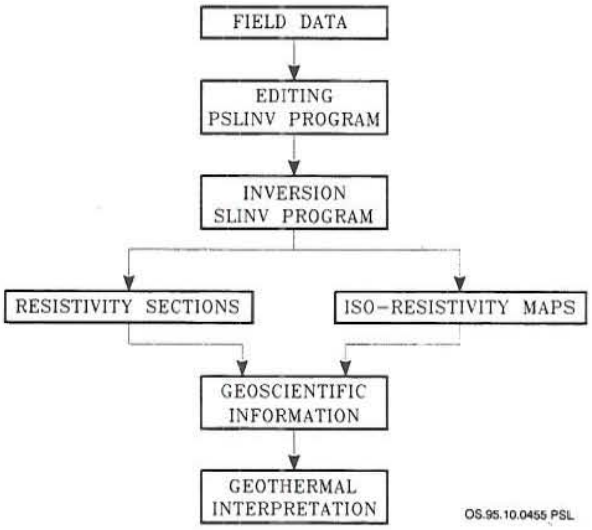

FIGURE 7: The one-dimensional interpretation process

Two-dimensional interpretation

Interpretation based on one-dimensional inversion programmes is inadequate when high resolution and detection of sharp resistivity boundaries is required. The main obstacle of the Schlumberger sounding is the sensitivity to relatively shallow lateral resistivity variations. The two-dimensional modelling of DC resistivity data, offers a substantial improvement in the resolution for the detection of vertical and lateral resistivity variations.

Two-dimensional modelling is achieved by using the FELIX programme, developed at Orkustofnun. This programme uses a finite element algorithm to evaluate the potential distribution in a two-dimensional resistivity distribution composed of triangular and rectangular resistivity blocks with infinite extension in the third dimension. FELIX is composed of two separate programmes, LIKAN and TULKUN, and can model cross-sections for up to ten sounding stations. LIKAN facilitates the construction of the two-dimensional resistivity model represented in the form of a grid, composed of triangular and rectangular resistivity blocks which are stored in an output file and processed later by TULKUN. TULKUN calculates the potential at the edges of the triangles by the finite element method, taking into consideration the relative position and the resistivity for each block, computing the resistivity values by simulating the actual electrode configuration. The calculated and measured apparent resistivity curves are compared and the interpreter decides how to adjust the model, running the programme repeatedly until a good fit is obtained.

4. DC RESISTIVITY SURVEY IN THE BERLÍN GEOTHERMAL FIELD

4.1 Field work

The field work was carried out from June to October 1994. Forty-one stations were measured with maximum AB/2 ranging from 1000 to 2000 m. The soundings are distributed in a regular grid with an average separation of one kilometre, crossing the geothermal area. Most of the soundings have a northeasterly direction and as such generally parallel to elevation iso-lines. The location of the soundings is shown in Figure 8. The resistivity curves and the results of one-dimensional interpretation, both the model and the corresponding curves are shown in Appendix I. The appendices to this report are published separately in a special data report (see Santos, 1995).

The equipment used were transmitters with generators, models TSQ-3 and TSQ-4 and one-channel analogical receivers, models IPR-8 and IPR-10 from Scintrex. The technical specifications are summarized in Tables 4 and 5 respectively.

The main limitation of the sounding data is the poor information on the inhomogeneities at shallow depth primarily because the overlap measured for each change of P was only two points. The soundings SEV19, SEV14, SEVTR7, and SEV06 seem to be strongly affected by shallow inhomogeneities. The

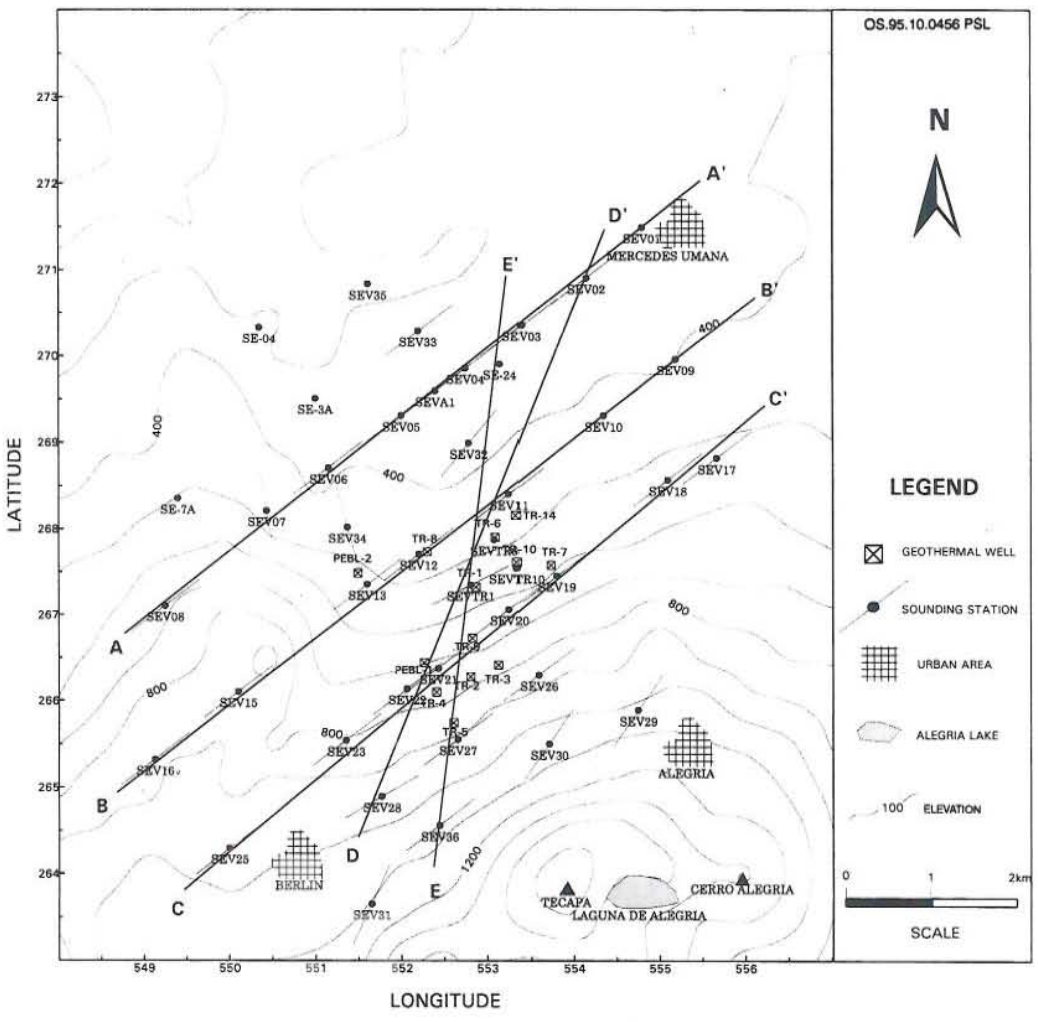

FIGURE 8: The location of resistivity soundings and cross-sections in the Berlín geothermal field

cables were frequently cut by animals, carts or due to friction with wire fences, which are numerous in this area. The cables were repaired and the repaired spot insulated with insulation tape, but that may come loose due to friction with the earth's surface. Thus, the repaired spots become leakage points for currents, especially in rain or even in damp weather. Current leakage can often be detected in the apparent resistivity curve and must be corrected in the field. Checks for current leakage should be made every now and then during the measurement of a sounding. Current leakage seems to have affected some of the soundings e.g. SEV10, SEV26, SEV27, SEVTR1 and SEVTR14. Another factor that seems to affect some of the field curves of the survey is the skin effect described in Section 3.3, mainly affecting soundings situated in the area of the low-resistivity anomaly. This happened especially in the readings taken when AB/2 was larger than 1000 m, where the signal in the receiver is weak and unstable, as observed in the SEV21, SEV22, and SEV13 soundings.

Due to the factors described above, as well as others described in Section 3.3, the SEVTR7, SEVTR14, SEVA2, SEV24, and SEV14 soundings were not used in the results. Instead, ten additional soundings, measured in the resistivity survey in 1977 in the northern part of the geothermal field, have been included in the results presented in the next section.

TABLE 4: Summary of the technical specifications of the transmitters used in the resistivity survey

Scintrex transmitter model	Voltage output range (V)	Maximum current output (A)	Reading resolution (mA)	Time domain pulse (s)	Motor generator (HP)	Shipping weight (kg)
TSQ-3	300-1500	10	10 (0-10 A)	1, 2, 4, 8, 16	8 HP	150
TSQ-4	500-3500	20	10 (0-20 A)	1, 2, 4, 8, 16, 32	25 HP	365

TABLE 5: Summary of the technical specifications of the receiver most used in the resistivity survey

Scintrex receiver model	Input impedance (Megaohm)	Primary voltage range (V)	Accuracy of Vp (full scale)	Low pass filters (db/oct)	Continuity metre range (kohms)
IPR-8	3	300 μV-40 V	3%	6	0-500

4.2 Results of one-dimensional interpretation

The results of the interpretation of 50 sounding stations, using the one-dimensional inversion programme SLINV, are presented in five resistivity cross-sections and iso-resistivity maps at five different levels. Figure 8 shows the location of the resistivity cross-sections.

4.2.1 Description of the resistivity cross-sections

Following is a brief description of each resistivity cross-section.

Cross-section AA' is trending in SW-NE direction, covering eight soundings (Figure 9). The features observed are:

a) A high-resistivity layer with values ranging between 150-5000 Ωm and an average thickness of

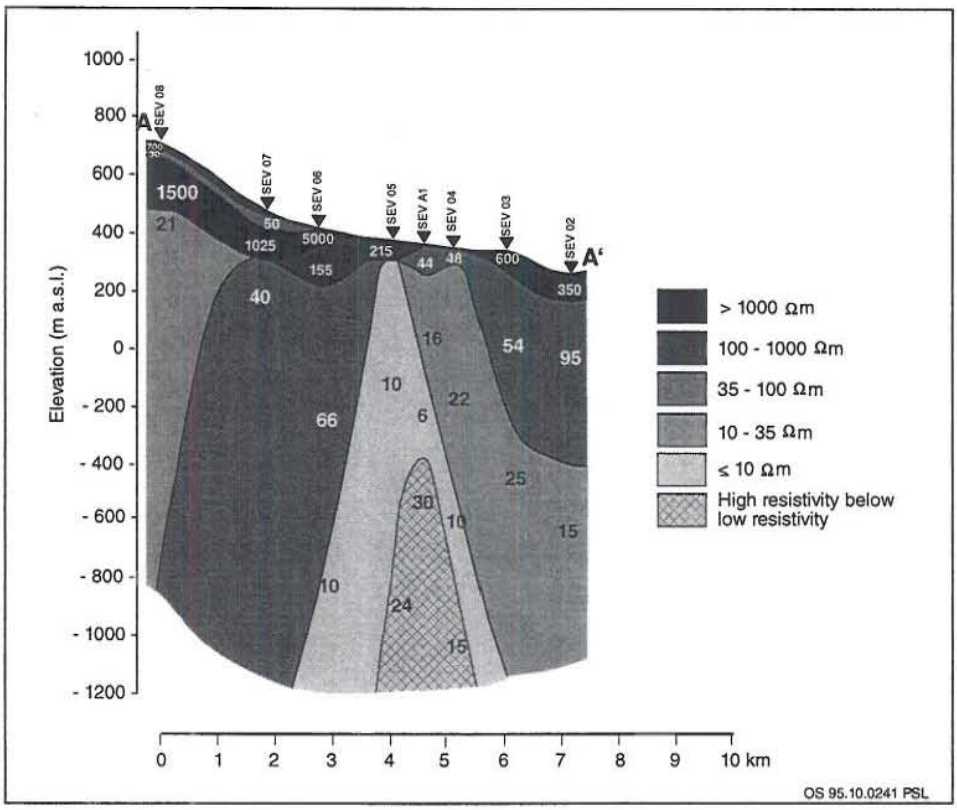

FIGURE 9: The Berlín geothermal field, resistivity cross-section A-A'

100 m at the top of the section;

b) A low-resistivity layer with values in the range of 5-10 Ωm in the central part like a coat over an inner high-resistivity layer or core;
c) A high-resistivity layer below the low resistivity cap with values of 15-30 Ωm, which appears at -400 m a.s.l. as a narrow inner core;
d) A flank layer around the low-resistivity cap with values in the range of 12-66 Ωm.

Cross-section BB' trending SW-NE includes seven soundings (Figure 10). The following aspects are observed:

a) A high-resistivity layer extending from the surface several metres down in the northeast up to a few hundred metres in the southwest;
b) A low-resistivity anomaly in the central part with values in the range of 4-8 Ωm, appearing again like a coat around a high-resistivity anomaly below;
c) A high-resistivity core extending up to an elevation of -60 m a.s.l.;
d) A high-resistivity layer (200 Ωm) appears in the uppermost 400 m in the northeastern part;
e) A high-resistivity layer appears in sounding SEV15, extending deep down. This is supported by the MT survey carried out in 1994 (GENZL, 1995). Other soundings show regional resistivity at depth in the range of 20-35 Ωm outside the actual high temperature field.

Cross-section CC' is parallel to the prior sections. It crosses the central part of the active geothermal area, where several geothermal manifestations are observed at the surface. Eight soundings are located on it (Figure 11). This cross-section has also been interpreted using two-dimensional modelling. The results of that will be presented and discussed in Section 4.3. The features observed are:

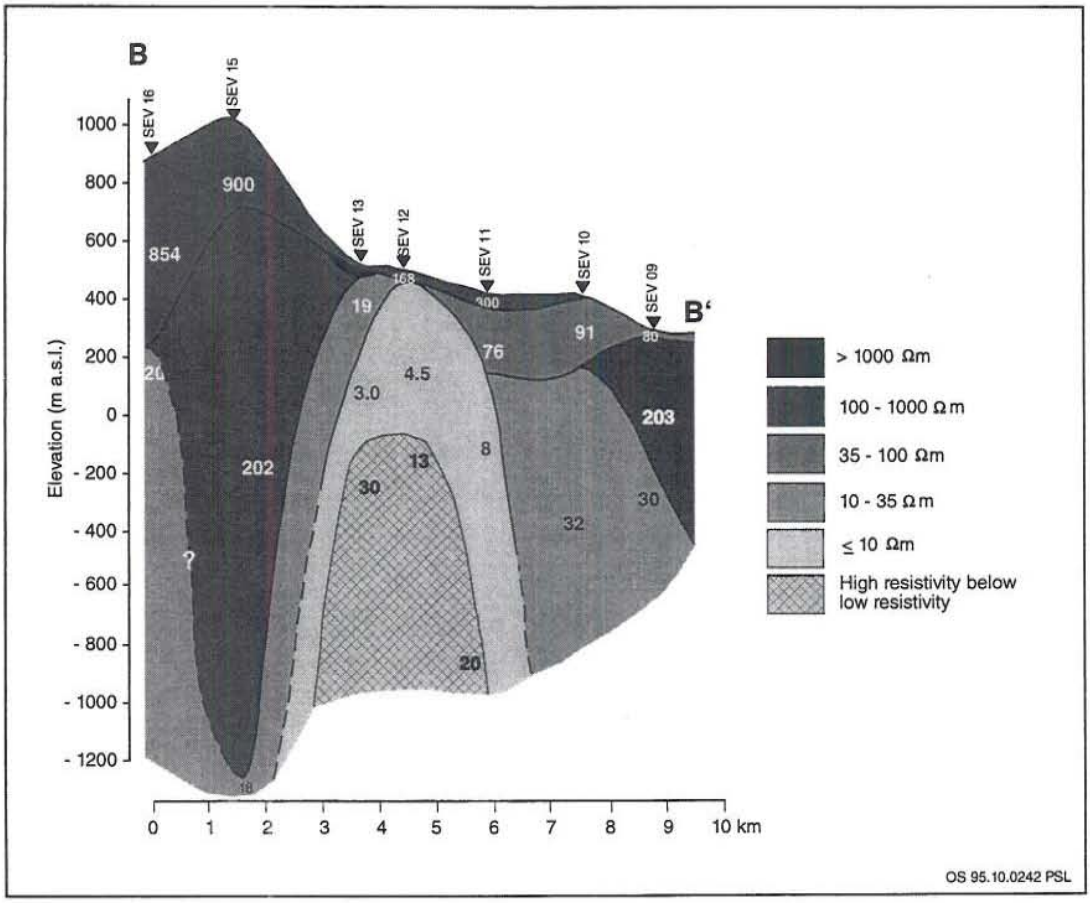

FIGURE 10: The Berlín geothermal field, resistivity cross-section B-B'

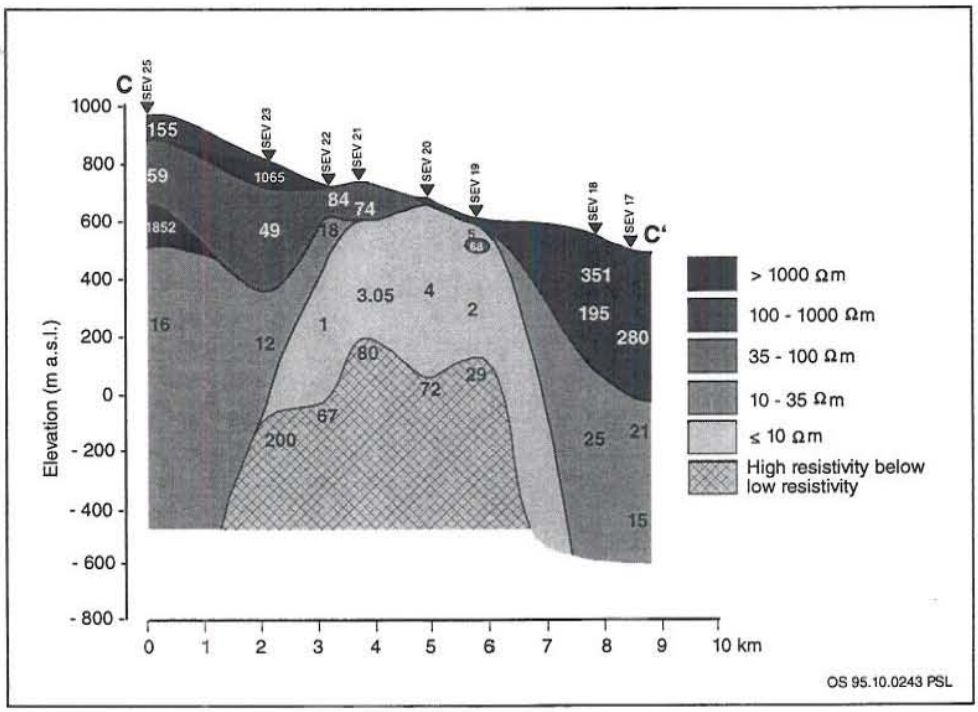

FIGURE 11: The Berlín geothermal field, resistivity cross-section C-C'

a) Outside the area of the main geothermal activity, a high-resistivity layer at the surface is extended down to 200 m depth with resistivity values from 150 to 1000 Ωm;
b) The low-resistivity cap with values less than 5 Ωm, extends close to the surface where the geothermal surface manifestations are seen;
c) The high-resistivity core below the low-resistivity cap is bigger and reaches higher with resistivity values from 30 to 200 Ωm. The resistivity values are not well defined and they are often based on only a few measured points;
d) The flank layers around the low-resistivity anomaly present lower resistivity values than in the previous cross-sections with resistivity values in the range of 12-25 Ωm;
e) The high-resistivity layer seen in the northeastern part of cross-section BB' is also seen here. The resistivity values range from 200-350 Ωm and the layer extends down to 500 m depth.

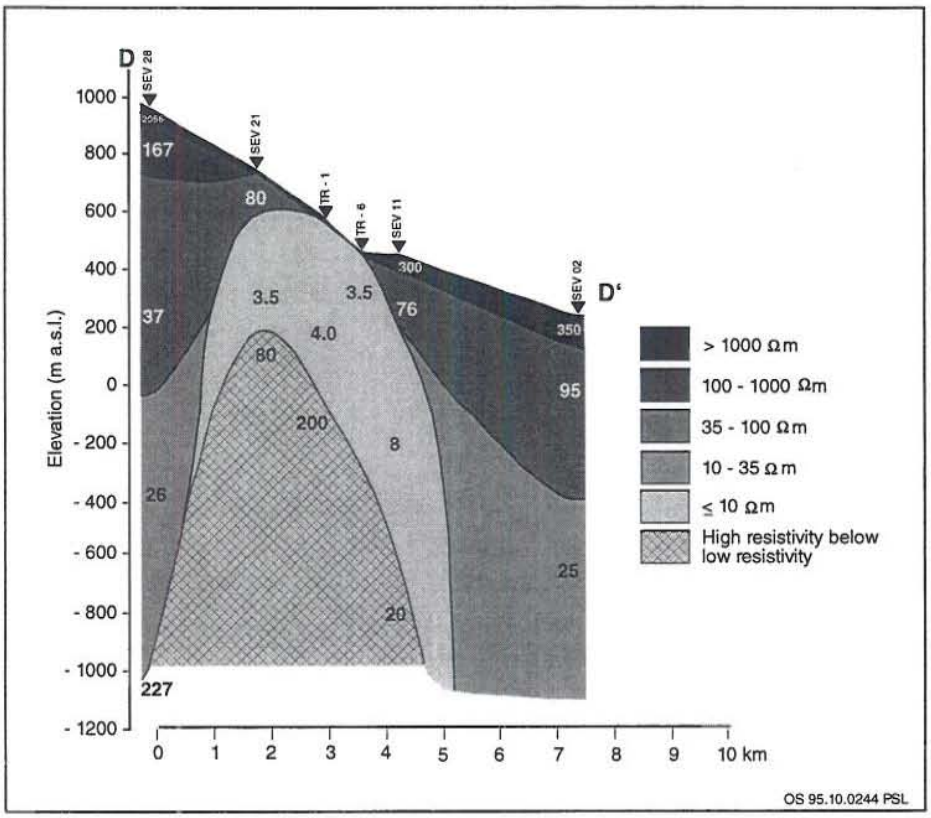

FIGURE 12: The Berlín geothermal field, resistivity cross-section D-D'

Cross-section DD' is 9 km long and is trending NNE-SSW. It is shown in Figure 12. The pattern observed in this section is similar to the previous ones, the features obtained are presented as follows:

a) The average thickness of the top high-resistivity layer (100-1000 Ωm) is less than 100 m;
b) The low-resistivity cap (3-8 Ωm), reaches surface in the central part of the profile where some hot springs and fumaroles are also observed ;
c) The high-resistivity core beneath the low-resistivity cap, extends to about 180 m a.s.l. in sounding SEV21, dipping drastically towards the north-northeast. It is observed at -700 m a.s.l. in sounding SEV11.
d) The low-resistivity anomaly is flanked by a resistivity layer of about 25 Ωm.

Cross-section EE' runs from north to south along the area where surface activity is most intense. It cuts through the first three cross-sections described above (Figure 13). The following aspects are observed in this profile:

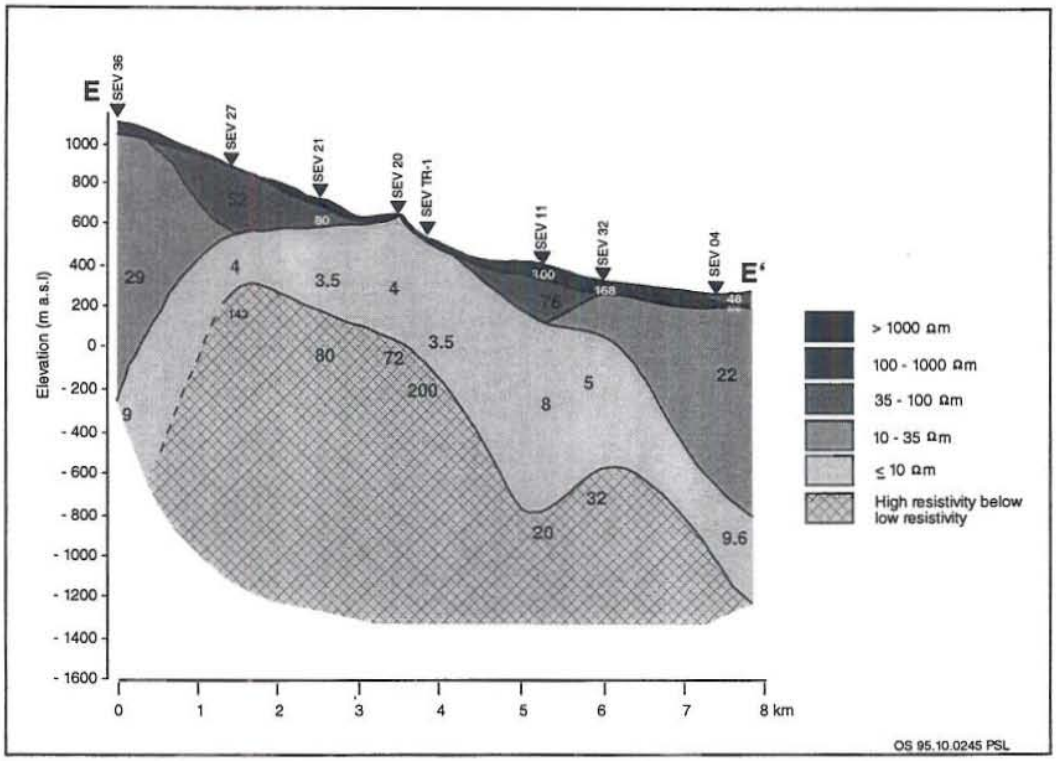

FIGURE 13: The Berlín geothermal field, resistivity cross-section E-E'

a) The shallow high-resistivity layer (100-1000 Ωm) at the surface is ranging in thickness from 50 to 100 m;
b) The low-resistivity cap in the profile has lower values (<5 Ωm) in the southern part of the section, and is observed at a shallow depth in this area;
c) The high-resistivity core rises up to 400 m a.s.l. in sounding SEV27, dipping clearly towards north with a downward dip in sounding SEV11. This is the highest elevation of the high resistivity core.

The main resistivity features in the cross-sections can be summarized as follows:

A high-resistivity **surface layer** (150-300 Ωm) extends from the surface to 400-500 m depth east of the geothermal field (cross-sections BB' and CC'). The resistivity values reach 1800 Ωm in the uppermost 200-600 m west and southwest of the high temperature field. Anomalously high resistivity at depth is seen in sounding SEV15, supported by results of a MT survey. **Regional resistivity** at depth, outside the high temperature field lies in the range of 20-35 Ωm. The high temperature field is clearly outlined with a **low-resistivity cap** with values less than 10 Ωm, underlain by a **high-resistivity core**. The low-resistivity cap reaches within a few metres of the surface, where surface manifestations are seen. The thickness of the low-resistivity cap is usually 500-600 m on top of the high-resistivity core, thinning as it dips down. The lowest resistivity values (<5 Ωm) are seen where the underlying high-resistivity core reaches elevation higher than -100 m a.s.l. The high-resistivity core has commonly values of 20-80 Ωm, but higher values are seen.

4.2.2 Iso-resistivity maps

A resistivity anomaly of a high-temperature field generally consists of very low resistivity values (<10 Ωm) and higher resistivity below the low-resistivity. Thus, the low-resistivity cap and the underlying

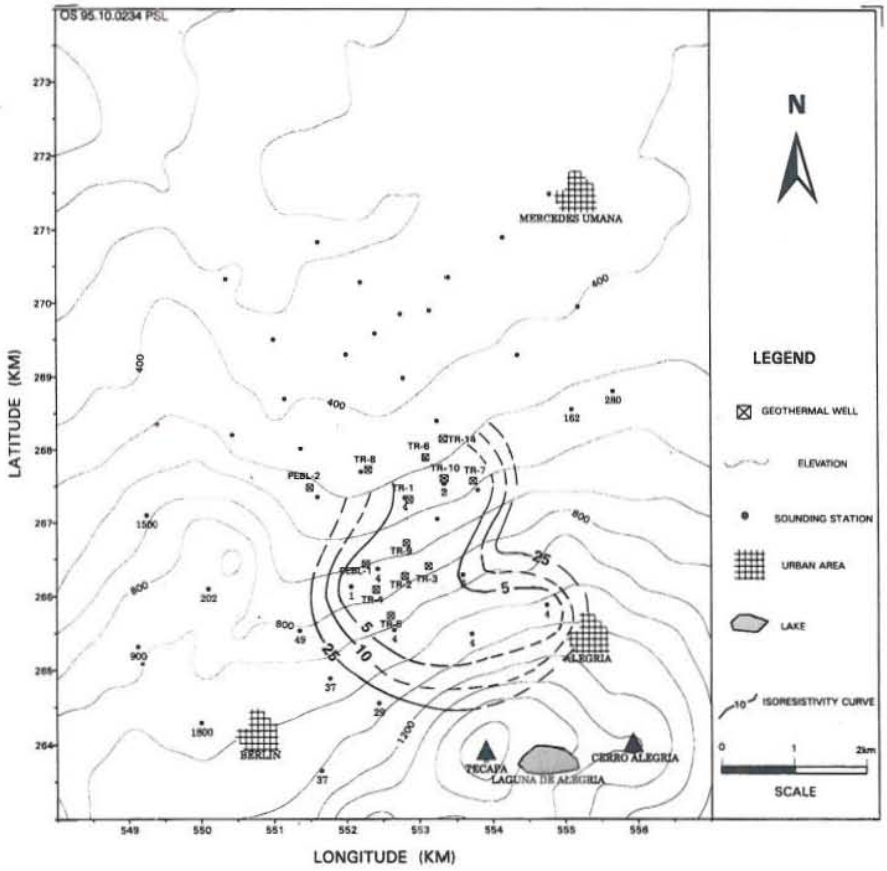

FIGURE 14: The Berlín field, iso-resistivity map at 500 m a.s.l.

high-resistivity core delineate the geothermal reservoir.

Figures 14-18 show iso-resistivity maps at 500, 250, 0, -250 and -500 m a.s.l. The resistivity values at the appropriate depth are shown for each sounding station. The iso-resistivity lines were drawn according to the resistivity models obtained from the one-dimensional inversion. Figure 17 shows the resistivity at -250 m a.s.l., the greatest depth at which all soundings give information on. This figure shows also the caldera faults and the main faults of the NNW-SSE trending fissure swarm as inferred in Figure 2.

In general the iso-resistivity maps show a low-resistivity anomaly within the caldera and extending to north-northwest into the NNW-SSE trending fissure swarm. The size of this anomaly increases with depth indicating an extensive geothermal system at depth. The main active area seems to be at the intersection between the NNW-SSE trending fissure swarm and the faults associated with the caldera collapse (caldera faults) as is clearly shown in Figure 17.

The high-resistivity core below the low-resistivity layer starts to appear at 400 m a.s.l. just south of the production area, trending NE-SW, at deeper levels. The size of this anomaly increases with depth and the trend changes towards the younger NNW-SSE fault system. This suggests that this system of faults may play an important role in the transportation of the geothermal fluids, i.e. it may act as an outflow zone. Supporting this is the location of some of the hot springs by a river in the NNE-SSW fissure swarm.

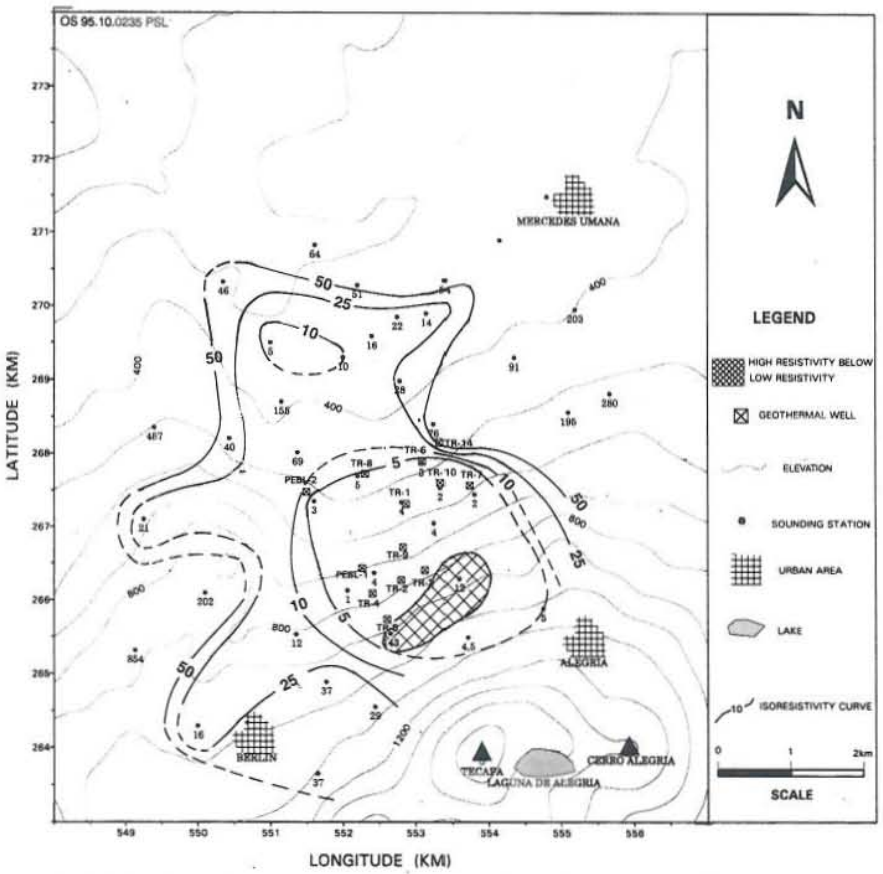

FIGURE 15: The Berlín field, iso-resistivity map at 250 m a.s.l.

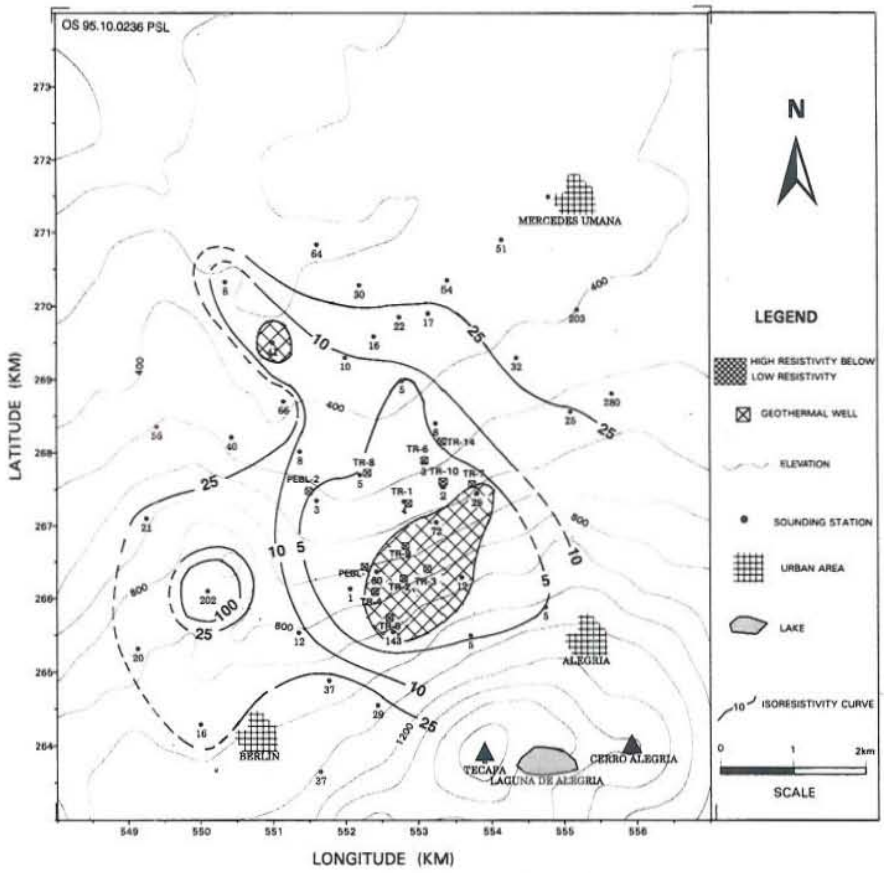

FIGURE 16: The Berlín field, iso-resistivity map at sea level

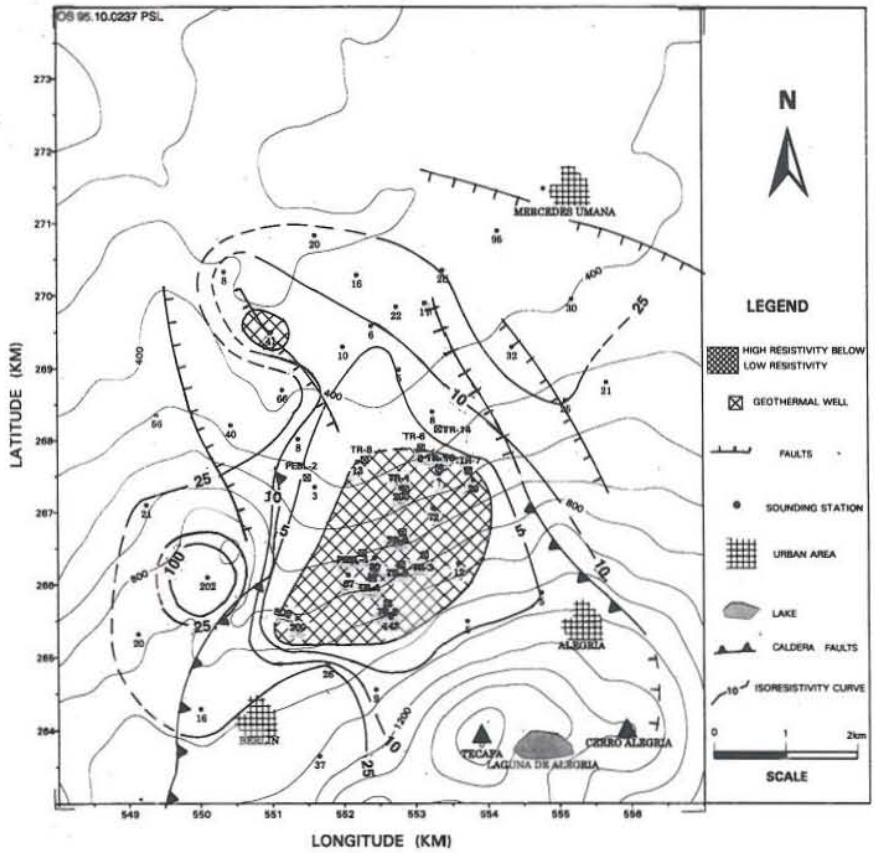

FIGURE 17: The Berlín field, iso-resistivity map at -250 m a.s.l.

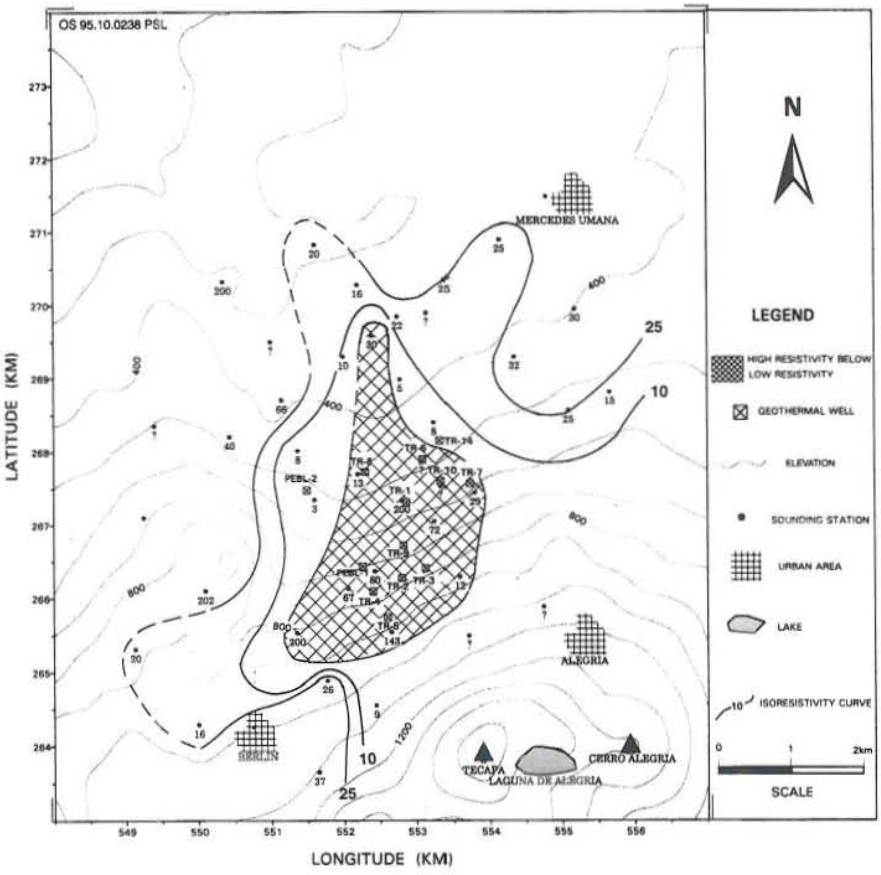

FIGURE 18: The Berlín field, iso-resistivity map at -500 m a.s.l.

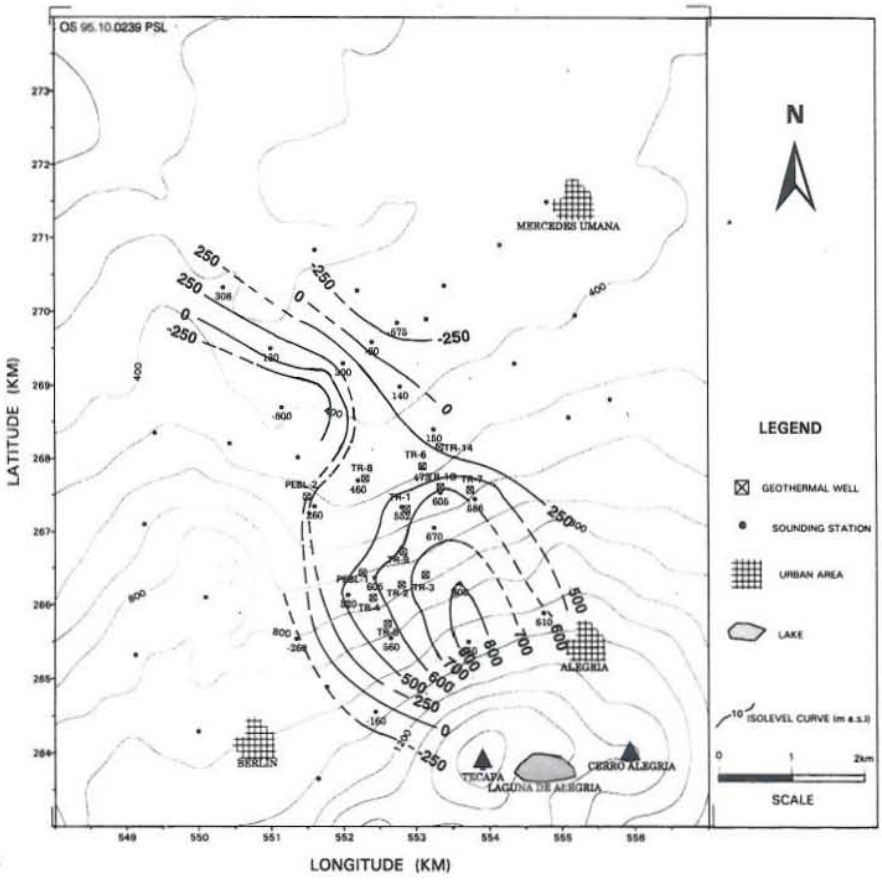

FIGURE 19: The Berlín field, elevation of the top of the low-resistivity cap (< 10 Ωm)

Figure 19 shows the elevation of the top of the low-resistivity cap (<10 Ωm), and Figure 20 the elevation of the top of the high-resistivity core. The high elevations registered in these figures for the low-resistivity cap and the high-resistivity core towards the southern part of the geothermal field suggest an upflow zone in this area. This is also supported by higher temperatures, and very low resistivity values in the low-resistivity cap.

4.2.3 Discussion of the results of one-dimensional interpretation

From the resistivity cross-sections and the iso-resistivity maps the following conclusions can be drawn:

1. The resistivity structure seen in the cross-sectionscan be classified into four resistivity layers; a) A high-resistivity layer at the surface outside the main active geothermal area, associated with the unaltered near-surface rocks above the ground water table; b) A low-resistivity cap with resistivity values in the range of 1-10 Ωm reflecting highly altered rocks. This will be discussed further later; c) A high-resistivity core below the low-resistivity cap caused by a change in the electrical conduction mechanism, from conductive layers with clay minerals on the surfaces in pores and fractures to more resistive layers with the crystalline structures of minerals like chlorite and epidote (Chapter 5); and d) A layer of relatively low resistivity (12-25 Ωm) flanking the resistivity anomaly, interpreted as a possible area of cooling because of a convective recharge (Georgsson et al., 1993). At further distance from the active geothermal field the resistivity lies in the range of 20-35 Ωm which reflects regional resistivity at depth.

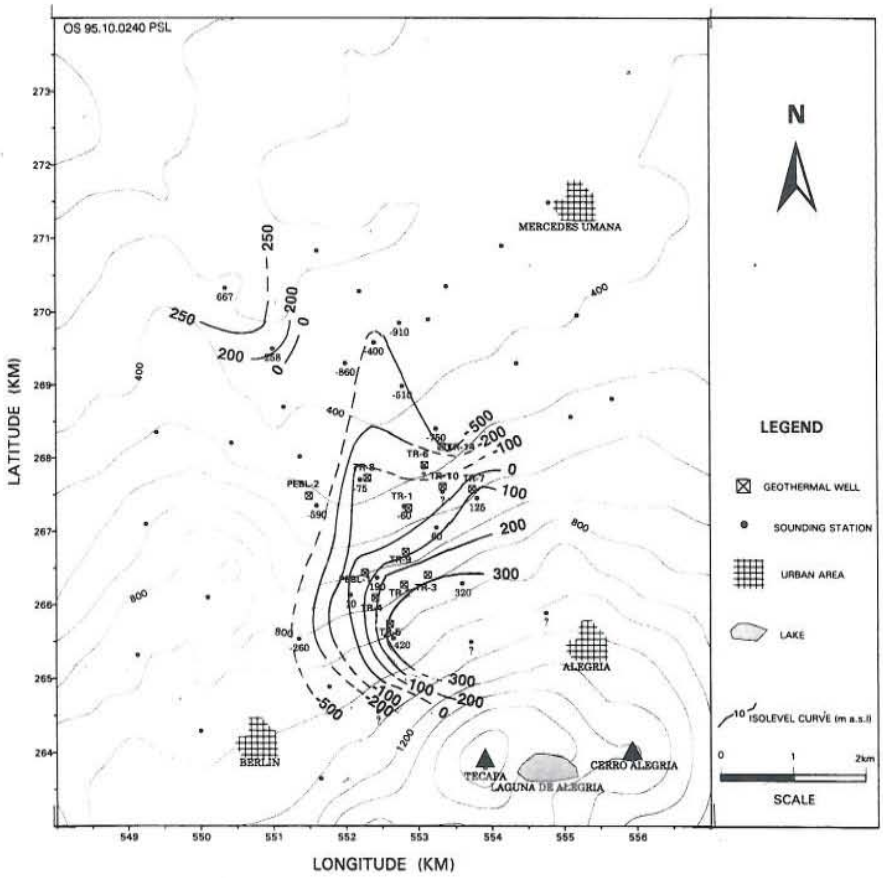

FIGURE 20: The Berlín field, elevation of the top of the high-resistivity core (>15 Ωm)

2. The iso-resistivity maps show an elongated low-resistivity anomaly trending NNW-SSE indicating an outflow zone along this fault system.
3. The maps showing the elevation of the top of the low-resistivity cap and the top of the high-resistivity core suggest an upflow zone in the southern part of the area which is also supported by high temperatures, and very low resistivity values in the cap.
4. Based on the iso-resistivity map at -250 m a.s.l. a geothermal field of 12 km^2 is delineated by the low-resistivity cap and the underlying high-resistivity core.

4.3 Two-dimensional interpretation, results and discussion

The application of two-dimensional modelling interpretation demands that the sounding stations are located along a profile nearly perpendicular to resistivity boundaries and in such a way that the current arms are kept in the same orientation, parallel or less than twenty degrees (20°) from the profile direction. The overlap of the current arms is desirable and an important help for identifying strong lateral variations.

According to these conditions, the profiles AA', BB' and CC' came into consideration for two-dimensional interpretation. However, only the CC' cross-section was chosen for the two-dimensional modelling, as it crosses the central part of the geothermal area which is of principal interest.

The two-dimensional model was set up for the CC' line based on the results from one-dimensional interpretation and the FELIX programme described in Section 3.4 used for interpretation. The results

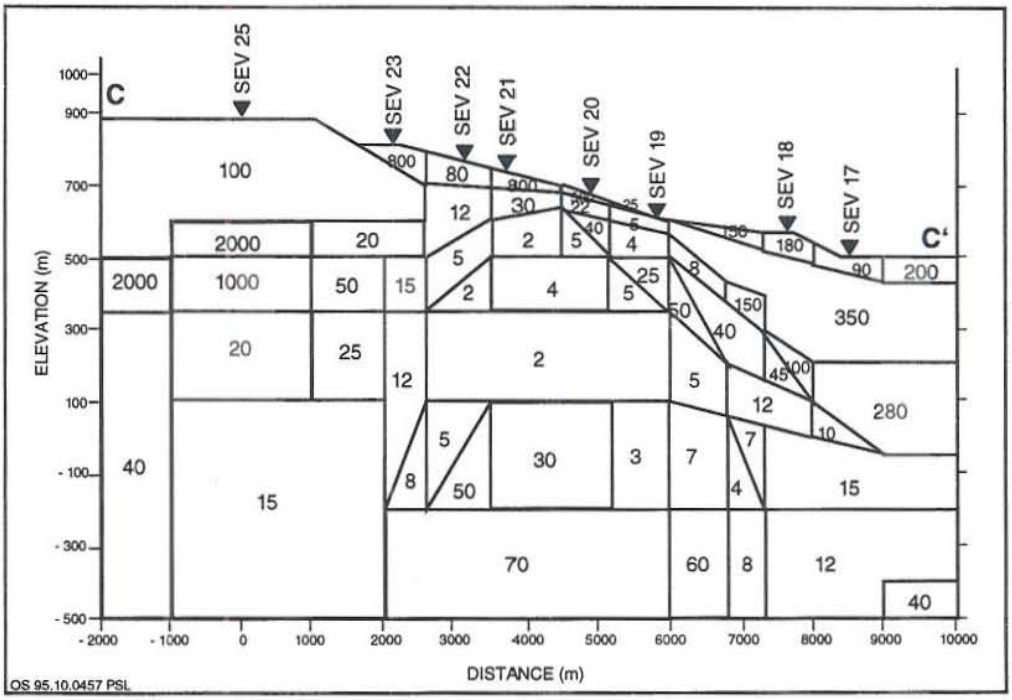

FIGURE 21: The Berlín geothermal field, two-dimensional model of resistivity cross-section C-C', the numbers in the blocks denote resistivity values in Ωm

of the modelling are shown in Figure 21 and a simplified model is presented in Figure 22. The resistivity curves and the curves corresponding to the response of the final two-dimensional model are presented in Appendix II (see Santos, 1995).

The results from two-dimensional analysis show a considerable improvement in the resolution of the soundings for the shallow lateral resistivity variations. From the comparison between the one and two-dimensional modelling for the CC' resistivity section the follows features are derived:

a) In general, a similar trending in the resistivity layers is observed in the results obtained from one-dimensional and two-dimensional modelling, showing the anomalous area located in the central part of the section;
b) The high-resistivity layer at the surface, associated with the unaltered rocks above the water table, has higher resistivity values and bigger thickness outside the zone of main geothermal activity;
c) The flank layer around the low-resistivity anomaly has in two-dimensional modelling lower values than obtained by one-dimensional interpretation.

The time demanded for the interpretation is considerably increased when the field data is affected by factors like described in Section 3.3. These factors must be eliminated in the field to avoid having "irregularities" in the resistivity curves that are due to technical problems. In this case two-dimensional and even three-dimensional interpretation would be required, increasing the time and cost of the interpretation work. This applies especially to soundings SEV25, SEV22 and SEV19, projected into this cross-section. The following discrepancies were noted:

a) The SEV25 sounding seems to be strongly affected by a shallow resistive body (2000 Ωm) observed much thicker than indicated by the one-dimensional modelling and it causes a sudden turn up in the measured curve. This high resistivity is underlain by a low-resistivity layer which is extended up the lateral vertical boundary under sounding SEV23 resulting in a steep change

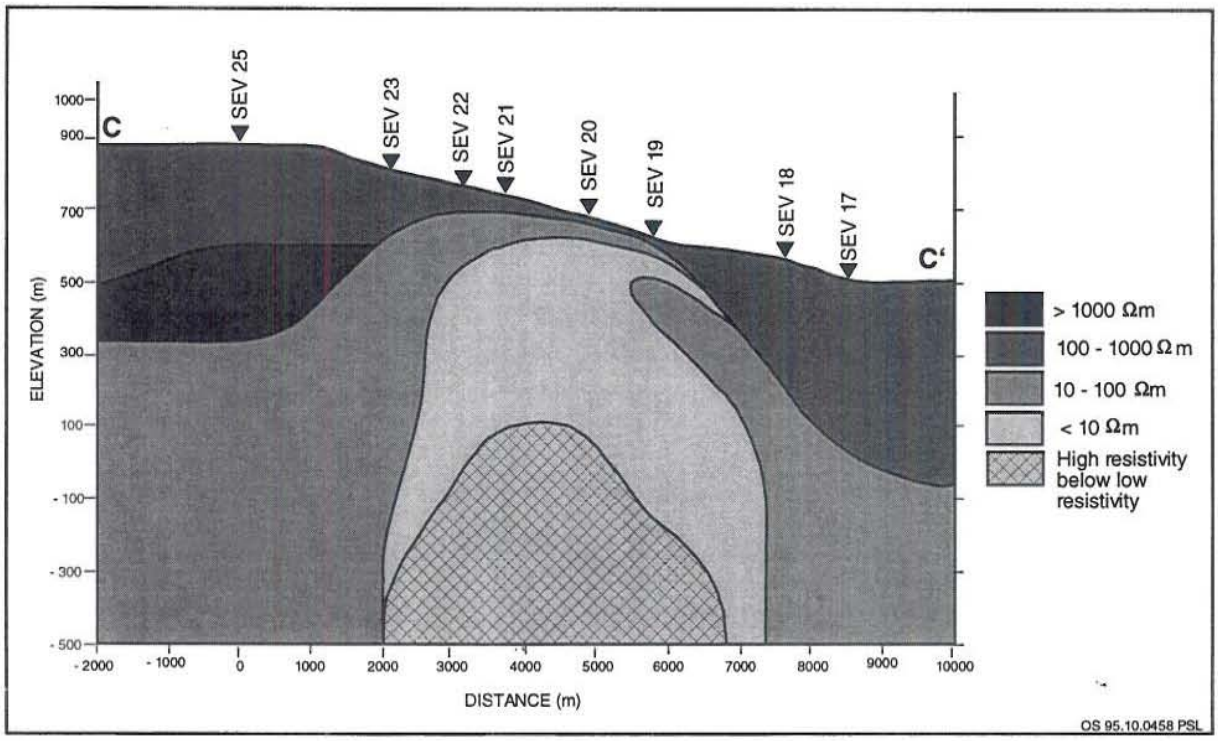

FIGURE 22: The Berlín geothermal field, simplified two-dimensional resistivity model of cross-section C-C'

upstream in the curve, which is difficult to fit well;

b) The vertical variation in the resistivity from the top layer to an anomaly with very low resistivity at depth produces an almost vertical fall in the field curve in SEV22 (from 80 to .5 Ωm), then a sudden upturn in the last segment in the curve is produced by the high-resistivity layer underneath the low-resistivity cap. This as well as three-dimensional effects can cause difficulties in obtaining a good fit between the calculated and measured curves;

c) According to the two-dimensional interpretation sounding SEV19 is situated over a low-resistivity layer and is being affected either by lateral and/or vertical shallow resistivity variations. There is observed a shallow high-resistivity body beneath the station. Due to the poor quality of the data it is impossible to decide what is the cause of the difference (200 m) in the prospection depth to the high-resistivity core in the one and two-dimensional modelling.

Soundings SEV23, SEV21, SEV20, SEV18 and SEV17, present a good correlation in depth and resistivity values with the results from one-dimensional modelling (see Appendix II, Santos, 1995).

5. CORRELATION WITH THE BOREHOLE DATA

5.1 Basaltic systems

A resistivity survey of a high-temperature field reflects the thermal alteration of the field, hence the temperature, providing there is an equilibrium between the thermal alteration and the temperature. This was clearly seen in the Nesjavellir high-temperature field in Iceland (Árnason and Hersir, 1993), when the results of one extensive resistivity survey were compared to borehole data showing a good correlation between the resistivity on one hand and the alteration and temperature on the other. High resistivity was

seen in fresh unaltered rocks at the surface. The resistivity decreased drastically in the smectite-zeolite zone in the temperature range 50-200°C. Only a minor alteration of basalt leads to the formation of a thin layer of clay minerals like smectite on the rock/water interface. These clay minerals have substantial cation exchange capacity, leading to an efficient electrical conduction in double layers between the clay minerals and the pore fluid. As a consequence, the bulk resistivity is almost independent of the pore fluid salinity in a fresh water geothermal reservoir. Elevated temperatures lead to increasing alteration as new alteration minerals are formed and others disappear.

At temperatures close to 250°C minerals like chlorite and epidote, which do not have high cation exchange capacity, substitute the clay minerals. As a consequence, the conduction mechanism changes from interface to electrolyte conduction above 250°C in fresh water systems, leading to increased resistivity (Flóvenz et al., 1985; Árnason and Flóvenz, 1992). This increase in resistivity is not as clear in systems with high salinity as the pore fluid conduction is dominant to the interface conduction both in the smectite-zeolite zone and in the chlorite zone (Georgsson, 1984; Flóvenz et al., 1985). The relation between alteration and temperature may also be different in saline systems as clay minerals are found at higher temperatures than in fresh water systems (Hrefna Kristmannsdóttir, pers. comm.).

5.2 Thermal alteration and resistivity in Berlín geothermal field

The above discussion on the resistivity and alteration may not convey directly to the Berlín high-temperature field. According to the cutting analysis, fresh basaltic rocks cover the uppermost 200-300 m in the boreholes, underlain by thermally altered rocks. Zoning may be different in a geothermal field with acidic rocks to that of a geothermal field with basaltic rocks as described in the above chapter.

The alteration zones in the Berlín geothermal field are described in Chapter 2.3. The argillic zone consists of zeolites and smectites (clay minerals) with the interface conduction as a dominant conduction mechanism. The argillic zone would correspond to the low-resistivity cap with resistivity values below 10 Ωm. The phyllic-argillic zone is a mixed layered clay zone and in the underlying phyllic-zone chlorite starts to appear and the clay minerals disappear.

The high-resistivity core observed in the resistivity survey appears within the phyllic-argillic zone, suggesting there is a change in the conduction mechanism. As stated before, chlorite is a resistive mineral appearing in the phyllic-zone. Another resistive mineral is sericite, a clay mineral also appearing in the phyllic-zone, sometimes at a higher elevation than the chlorite (IIE, 1992). It is therefore concluded that the change in the conduction mechanism and the increase in the resistivity occur in the transition zone (phyllic-argillic) between the high conductive argillic zone (smectite and zeolite) and the resistive phyllic-zone (chlorite and sericites).

In order to compare the results of the resistivity survey to borehole data (Figure 23), the geothermal wells TR-5, TR-2, TR-9 and TR-14 have been projected onto the cross-section EE'. The borehole data obtained from these wells include the alteration zoning obtained from the secondary mineralogy and the measured formation temperature.

There is good correlation between the resistivity and the thermal alteration in the southern part of the field (wells TR-5, TR-2 and TR-9). The formation temperature has been derived from the temperature logs in the wells, showing the same trend as the resistivity i.e. highest temperatures in well TR-5, where the high-resistivity core reaches highest elevation. This suggests an upflow zone in the near vicinity of well TR-5.

The good correlation between resistivity and alteration in the southern part of the wellfield is not evident

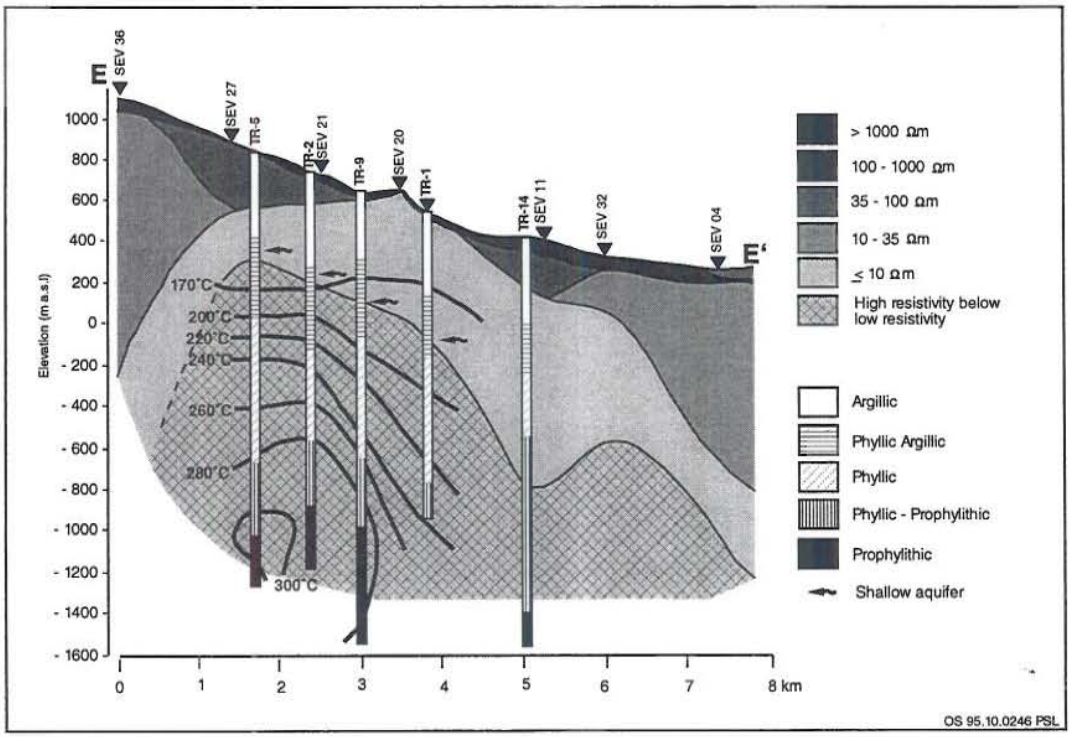

FIGURE 23: Resistivity cross-section E-E' correlated with borehole data

in well TR-14 in the northern part. There is an indication of cooling towards north in the temperature logs (in well TR-1) and in the alteration study made by IIE (1992), an abundance of low temperature zeolites were found in well TR-1, suggesting cooling in this area. A downward dip is observed in the high-resistivity core in sounding SEV11 close to well TR-14. This resistivity boundary is not well defined at such depths, but the low-resistivity cap is clearly thicker and has a higher resistivity value. Temperature logs from well TR-14 were not available.

Thermal alteration zoning in wells TR-1 and TR-14 would indicate higher temperatures than obtained by logging. The difference in the measured temperature in well TR-1 and the resistivity soundings could possibly be explained as follows. The thermal alteration is formed at an earlier stage in the thermal history of this area, when higher temperatures were present. Then cooling occurs as indicated by the temperature logs and low-temperature zeolites overprint the high temperature alteration, sufficiently to affect the conduction and thus the results of the resistivity measurements.

The formation temperature in the reservoir seems to be higher than expected from the thermal alteration (see Table 3), especially in the phyllic-prophylithic and prophylithic zone. This could mean that the upflow zone in the southern part of the wellfield is warming up. It must, however, be kept in mind that thermal alteration zoning in a high-temperature field in basaltic environment may not convey exactly to that of a high-temperature field in silicic environment. It has also been observed that clay mineralogy and temperatures of clay conversions are different in geothermal systems with brine waters than in fresh water systems (Kristmannsdóttir, 1985). The existence of a high-resistivity core in the Berlín field shows that it would be defined as a fresh water system, at least in the uppermost km of the field, the part delineated by the resistivity soundings.

6. CONCLUSIONS AND RECOMMENDATIONS

The main conclusions derived from this work are summarized as follows:

1. The Berlín high-temperature field is located at the intersection between the Berlín caldera faults and the NNE-SSW trending fissure swarm;

2. The high-temperature field shows clear features with a low-resistivity cap (resistivity values ≤ 10 Ωm) underlain by a high-resistivity core (20-80 Ωm). The thickness of the low-resistivity cap is usually 500-600 m in the centre, thinning as it dips down. The lowest resistivity values (<5 Ωm) are seen where the underlying high-resistivity core reaches elevation higher than -100 m a.s.l., within the caldera in the southern part of the geothermal field;

3. The resistivity survey reveals an extensive geothermal field which is 12 km^2 at -250 m a.s.l. as indicated by a low-resistivity cap and an underlying high-resistivity core;

4. The high-resistivity core delineates a high-temperature reservoir with temperatures exceeding 230°C providing there is an equilibrium between temperature and alteration;

5. The upflow zone is within the caldera close to well TR-5, supported by the highest temperatures, highest elevations of the high-resistivity core, and lowest resistivity values in the low-resistivity cap;

6. A high-resistivity surface layer outside the geothermal field corresponds to fresh cold rocks, with decrease in resistivity below the water table;

7. The existence of a high-resistivity core suggests a fresh water system in the uppermost part of the reservoir, i.e. in the part probed into by the resistivity soundings;

8. An outflow zone into the north-northwesterly fissure swarm is suggested by the north-northwesterly trending resistivity anomaly as shown in the iso-resistivity maps;

9. A good correlation is seen between the resistivity survey, the thermal alteration and formation temperature derived from temperature logs in the southern part of the wellfield. A possible upwarming is suggested at depths in the upflow zone within the caldera, close to well TR-5;

10. There is an indication of a cooling area in the northern part of the wellfield in the vicinity of wells TR-1 and TR-14. This is supported by the temperature logs and the resistivity survey;

11. There is no obvious correlation between the lithologic structure and the different resistivity layers obtained from the one-dimensional interpretation;

12. A considerable improvement in the resolution of the soundings is obtained by the two-dimensional analysis especially for the shallow lateral resistivity variations, and defining vertical resistivity boundaries. Considering the high cost and low probability of a successful drilling of a well it should encourage geothermal planners to use two-dimensional modelling as a standard interpretation method;

13. For the best results of a resistivity survey and the following often time consuming interpretation careful data acquisition is required.

ACKNOWLEDGEMENTS

I would like to express my gratitude to Dr. Ingvar B. Fridleifsson, Director of UNU Geothermal Training Programme for giving me the opportunity to participate in this special course; to Mr. Lúdvík S. Georgsson, Ms. Súsanna and Margrét Westlund for their efficient help and kindness during the training course, to Ms. Helga B. Sveinbjörnsdóttir and the drawing office staff for drawing and preparing figures for this report.

Great thanks to Ragna Karlsdóttir, my adviser, for sharing her knowledge and experience in geothermal interpretation of resistivity methods, assistance and supervising this work. Thanks to UNU lecturers and Orkustofnun staff for sharing their knowledge, especially to Knútur Árnason for his patient guiding through the special geophysics lectures and the critical review of the theoretical part of this report.

I would like also to thank the Comision Eléctrica del Río Lempa (CEL), the Superintendencia de Evaluacion de Recursos Geotérmicos and El Departamento de Investigaciones Geocientíficas for giving me the opportunity to attend this course and supplying me with the information used in this report

My deep gratefulness to my family, specially my wife Carmen Adela and my daughter Kelly Beatríz for giving me their spiritual support during the six long months of physical separation.

REFERENCES

Árnason, K., 1984: The effect of finite electrode separation on Schlumberger soundings. *54th Annual International SEG Meeting, Atlanta, Ga., Expanded Abstracts*, 129-132.

Árnason, K., 1993: Relation bewteen resistivity and geothermal activity in basaltic rocks. English translation of a chapter in: *Geothermal activity at the Ölkelduháls field, resistivity soundings in 1991 and 1992.* Orkustofnun, Reykjavík, report OS-93037/JHD-10 (in Icelandic), 82 pp.

Árnason, K., and Flóvenz, Ó.G., 1992: Evaluation of physical methods in geothermal exploration of rifted volcanic crust. *Geoth. Res. Council, Transactions, 16,* 207-214.

Árnason, K., and Hersir, G.P., 1988: *One-dimensional inversion of Schlumberger resistivity soundings. Computer program, description and user's guide.* UNU G.T.P., Iceland, report 8, 59 pp.

Benito, F.A., 1991: *Interpretation of Schlumberger soundings from Mt.Cagua, Philippines and TEM soundings from Svartsengi-Eldvörp, SW-Iceland.* UNU G.T.P., Iceland, report 4, 42 pp.

CEL, 1991: *Superficial geochemistry synthesis of the Berlin geothermal field.* CEL - Comisíon Ejecutiva Hidroeléctrica del Rio Lempa, internal report (in Spanish).

ELC, 1993: *Resource evaluation of the Berlín geothermal field, final version.* Electroconsult, internal report CGB-2-ELC-R-11994(R01) (in Spanish), submitted to CEL.

Flóvenz, Ó.G., 1984: Application of the head-on resistivity profiling method in geothermal exploration. *Geoth. Res. Council, Transactions, 18,* 493-498.

Flóvenz, Ó.G., Georgsson, L.S., and Árnason, K., 1985: Resistivity structure of the upper crust in Iceland. *J. Geophys. Res., 90-B12,* 10136-10150.

GENZL, 1995: *The Berlín geothermal field, geoscientific studies; part 6, integrated report.* Geothermal Energy New Zealand Ltd., report (in Spanish) submitted to CEL, 29 pp.

Georgsson, L.S., 1984: Resistivity and temperature distribution of the outer Reykjanes Peninsula, Southwest Iceland. *54th Annual International SEG Meeting, Atlanta, Ga., Expanded Abstracts*, 81-84.

Georgsson, L.S., Árnason, K., and Karlsdóttir, R., 1993: Resistivity sounding in high temperature areas in Iceland, with examples from Öxarfjördur, N-Iceland and Brennisteinsfjöll, SW-Iceland. *14th PNOC-EDC Geothermal Conference, Manila, Philippines*, 9 pp.

Hersir, G.P., and Árnason, K., 1989: *Schlumberger soundings over a horizontally stratified earth. Theory, instrumentation and user's guide to the computer programme ELLIPSE.* UNU G.T.P., Iceland, unpublished report.

Hersir, G.P., and Björnsson, A., 1991: *Geophysical exploration for geothermal resources, principles and application.* UNU G.T.P., Iceland, report 15, 94 pp.

Hochstein, M.P., Risk, G.F., and Caldwell, 1982: *Introduction to geothermal prospecting.* University of Auckland, Geothermal Institute, unpublished lectures.

IIE, 1992: *Petrological studies of the Berlín geothermal field, El Salvador C.A.* Internal report (in Spanish), Instituto de Investigaciones Electricas, 24 pp + 55 figures and appendix.

Koefoed, O., 1979: *Geosounding principles, 1. Resistivity sounding measurements.* Elsevier Scientific Publishing Co., Amsterdam, 276 pp.

Kristmannsdóttir, H., 1978: Alteration of basaltic rocks by hydrothermal activity at 100-300°C. In: Mortland, M.M., and Farmer, V.C. (editors), *International Clay Conference 1978.* Elsevier Scientific Publishing Co., Amsterdam. 359-367.

Kristmannsdóttir, H., 1985: The role of clay minerals in geothermal energy research. *Proceedings of the Nordic Symposium: Clay Minerals - Modern Society, Uppsala, Nov. 1985,* 125-131.

Monterrosa V., M.E., 1993: *A 3-D natural state modelling and reservoir assessment for the Berlín geothermal field in El Salvador, C.A.* UNU G.T.P., Iceland, report 11, 45 pp.

Pullinger, C.R., and Barrios L., L., 1994: *Evaluation of geoscientific information from wells TR-8 and TR-14 Berlín geothermal field.* CEL, internal report (in Spanish), 19 pp.

Pullinger, C.R., and Bruno, C.E., 1995: *Exploration and development of geothermal resources for power generation in El Salvador.* CEL, internal report.

Quijano C., J.E., 1994: A revised conceptual model and analysis of production data for the Ahuachapan-Chipilapa geothermal field in El Salvador. Report 10 in: *Geothermal Training in Iceland 1994.* UNU G.T.P., Iceland, 237-266.

Reyes V., P., 1989: *Resistivity methods with application to Planillas geothermal field, Mexico.* UNU G.T.P., Iceland, report 9, 56 pp.

Santos L., P.A., 1995: *Appendices to the report: One- and two-dimensional interpretation of DC-resistivity data from the Berlín geothermal field, El Salvador.* UNU G.T.P., Iceland, report 11 appendices, 15 pp.

Ward, S.H., and Sill, W.R., 1983: *Resistivity, induced polarization, and self-potential methods in geothermal exploration.* UNU G.T.P., Iceland, report 3, 94 pp.

Weyl, R., 1980: *Geology of Central America.* 2nd completely revised edition, Gebruder Borntraeger, Berlin-Stuttgart, 371 pp.